2023

Design, Synthesis And Biological Evaluation Of A Novel Bioactive Indane scaffold 2-(diphenylmethylene)c-2,3-dihydro-1H-inden-1-one with potential anticancer activity

Tao Zhang
Technological University Dublin, Ireland, tao.zhang@tudublin.ie

Vilmar Bandero
Trinity College Dublin, Ireland

Claire Corcoran
Trinity College Dublin, Ireland

See next page for additional authors

Funder: This work was supported by Trinity College Dublin Postgraduate Scholarships.

European Journal of Pharmaceutical Sciences 188 (2023) 106529

Contents lists available at ScienceDirect

European Journal of Pharmaceutical Sciences

journal homepage: www.elsevier.com/locate/ejps

Design, synthesis and biological evaluation of a novel bioactive indane scaffold 2-(diphenylmethylene)c-2,3-dihydro-1H-inden-1-one with potential anticancer activity

Tao Zhang [a,b,c,*,1], Vilmar Bandero [c,1], Claire Corcoran [c], Ismael Obaidi [b,d], Manuel Ruether [e], John O'Brien [e], Lorraine O'Driscoll [c], Neil Frankish [c], Helen Sheridan [b,c,*]

[a] School of Food Science and Environmental Health, Technological University Dublin, Grangegorman, Dublin 7, D07 ADY7, Ireland
[b] The Trinity Centre for Natural Products Research (NatPro), School of Pharmacy and Pharmaceutical Sciences, Trinity College Dublin, Dublin 2, D02 PN40, Ireland
[c] Drug Discovery Group, School of Pharmacy and Pharmaceutical Sciences and Trinity Biomedical Sciences Institute, Trinity College Dublin, Dublin 2, D02 PN40, Ireland
[d] College of Pharmacy, University of Babylon, Babylon, Iraq
[e] School of Chemistry, Trinity College Dublin, Dublin 2, Ireland

ARTICLE INFO

Keywords:
Indanone
Benzophenones
Anticancer
In vitro cytotoxicity
Cell cycle analysis

ABSTRACT

Over the past decades, designing of privileged structures has emerged as a useful approach to the discovery and optimisation of novel biologically active molecules, and many have been successfully exploited across and within different target families. Examples include indole, quinolone, isoquinoline, benzofuran and chromone, etc. In the current study, we focus on synthesising a novel hybrid scaffold constituting naturally occurring benzophenone (**14**) and indanone (**22**) ring systems, leading to a general structure of 2-(diphenylmethylene)-2,3-dihydro-1H-inden-1-one (**23**). It was hypothesised this new hybrid system would provide enhanced anti-cancer activity owing to the presence of the common features associated with the tubulin binding small molecule indanocine (**10**) and the estrogen receptor (ER) antagonist tamoxifen (**24**). Key hybrid molecules were successfully synthesised and characterised, and the *in vitro* cytotoxicity assays were performed against cancer cell lines: MCF7 (breast) and SKBR3 (breast), DU145 (prostate) and A549 (lung). The methyl-, chloro- and methoxy-, *para*-substituted benzophenone hybrids displayed the greatest degree of cytotoxicity and the *E*-configuration derivatives **45, 47** and **49** being significantly most potent. We further verified that the second benzyl moiety of this novel hybrid scaffold is fundamental to enhance the cytotoxicity, especially in the SKBR3 ($HER2^+$) by the *E*-methyl lead molecule **47**, MCF7 (ER^+) by **45** and **49**, and A549 (NSCLC) cell lines by **49**. These hybrid molecules also showed a significant accumulation of SKBR3 cells at S-phase of the cell cycle after 72 hrs, which demonstrates besides of being cytotoxic *in vitro* against SKBR3 cells, **47** disturbs the replication and development of this type of cancer causing a dose-dependent cell cycle arrest at S-phase. Our results suggest that DNA damage might be involved in the induction of SKBR3 cell death caused by the hybrid molecules, and therefore, this novel system may be an effective suppressor of HER2+/Neu-driven cancer growth and progression. The present study points to potential structural optimisation of the series and encourages further focussed investigation of analogues of this scaffold series toward their applications in cancer chemoprevention or chemotherapy.

1. Introduction

The indane scaffold (**1**) is of key importance in medicinal chemistry. It occurs in a range of natural products that have been isolated from organisms that occur at different evolutionary levels in the plant kingdom. Indane metabolites have been isolated from natural resources include simple indanone (**2**) from the cyanobacterium *Nostoc* (Jaki et al., 1999), tripartin (**3**) from the culture broth of the *Streptomyces* sp. associated with a larva of the dung beetle *Copris tripartitus* (Kim et al., 2013), the illudalane sesquiterpenes granulolinden A (**4**) and

* Corresponding authors.
E-mail addresses: tao.zhang@TUDublin.ie (T. Zhang), banderv@tcd.ie (V. Bandero), corcorcl@tcd.ie (C. Corcoran), obaidii@tcd.ie (I. Obaidi), ruetherm@tcd.ie (M. Ruether), jeobrien@tcd.ie (J. O'Brien), lodrisc@tcd.ie (L. O'Driscoll), nfrnkish@tcd.ie (N. Frankish), hsheridn@tcd.ie (H. Sheridan).
[1] These authors contributed equally.

https://doi.org/10.1016/j.ejps.2023.106529
Received 8 February 2023; Received in revised form 23 June 2023; Accepted 14 July 2023
Available online 17 July 2023

dihydrogranuloinden (**5**) from the basidiomycete *Granulobasidium* (Nord et al., 2014), trikentramine (**6**) from *Trikentrion loeve* (Coyanis et al., 2006), ampelopsin D (**7**) from *Ampelopsis grossedentata* (Kou et al., 2012). There are many indane derived compounds in development for their significant broad therapeutic properties and some are in clinical use, including anti-inflammatory [e.g. sulindac (**8**)] (Lant, 1981), antiviral (e.g. CCR5 antagonist **9**) (Xue et al., 2010), anticancer [e.g. indanocine (**10**)] (Leoni et al., 2000) activities (Fig. 1a). Several classes of indane-based compounds (**11a-c, 12a-c** and **13a-f**) have been developed and investigated by our research group for various conditions, such as smooth muscle relaxation, mediator release inhibition and inflammatory conditions (Chan et al., 2020; Frampton et al., 2012; Frankish et al., 2004; Frankish and Sheridan, 2012; Frankish et al., 2017; Sheridan et al., 2009; Zhang et al., 2015) (Fig. 1a).

Benzophenones, a class of natural compounds consisting of more than 300 members, are also found in a number of edible or medicinal species, mainly in the Clusiaceae family which exhibit great structural diversity but share a common ketone skeleton (**14**), (Ferraz et al., 2021; Wu et al., 2014). Benzophenones are important compounds in organic synthesis and have been used as starting materials for the preparation of various drugs. The biphenyl benzophenone structure (**14**) and its modified forms have been found in 4.3% of all known drugs. (Hajduk et al., 2000) Many of these natural benzophenones and synthetic benzophenone-derived molecules have been shown to exhibit a range of biological activities, including antioxidant (e.g. **15**) (Zou et al., 2023), anti-parasitic [e.g. **16** (LFQM-123)] (Maciel-Rezende et al., 2013), antiviral [e.g. **17** (GW678248)] (Ferris et al., 2005), anti-inflammatory [e.g. **18**] (Zeng et al., 2022), anti-proliferative and cytotoxic [e.g. **19** and phenstatin (**20**)], (Biljali et al., 2013; Pettit et al., 1998) and cholinesterase inhibition as possible treatment for Alzheimer's condition [e.g., 21] (Godyń et al., 2022) (Fig. 1b).

Although both indane [and related indanone (**22**), indene and indanol] and benzophenone ring systems occur in naturally derived and synthetic molecules, they have not been described in the literature as privileged structures in the field of medicinal chemistry. In the current study we focus on the synthesis of a novel hybrid scaffold with the new general structure **23** [2-(diphenylmethylene)-2,3-dihydro-1H-inden-1-one] constitutes of these two nature derived ring systems: indanone and benzophenone (Scheme 1) and bio-evaluation of its anticancer activities. The hybrid was designed with the aim of incorporating cytotoxicity into the new structures *via* tubulin binding properties as seen in indanocine (**10**) and phenstatin (**20**). We also anticipate that the novel hybrid may exhibit estrogen receptor (ER) antagonism properties derived from the structural similarity of the new scaffold to tamoxifen (**24**) (Fig. 2).

2. Materials and methods

2.1. Synthesis and characterisation

All reagents were commercially available from Sigma Ireland and were used without further purification unless otherwise indicated. TLC analysis was performed using Merck Silica gel 60 TLC aluminium sheets with fluorescent indicator visualising with UV light at 254 nm. Flash chromatography was carried out using Merck silica gel 60 (230–400 mesh) and visualisation was by examination under UV light at 254/365 nm and/or by spraying with p-anisaldehyde staining reagent. All products isolated were homogenous on TLC. NMR experiments were acquired at 27°C on a Bruker DPX 400 spectrometer (400.13 MHz for ^{1}H; 100.61 MHz for ^{13}C) in $CDCl_3$ [internal standard, tetramethylsilane (TMS)]. For $CDCl_3$, ^{1}H NMR spectra were assigned relative to the tetramethylsilane (TMS) peak at 0.00 ppm, and ^{13}C NMR spectra were

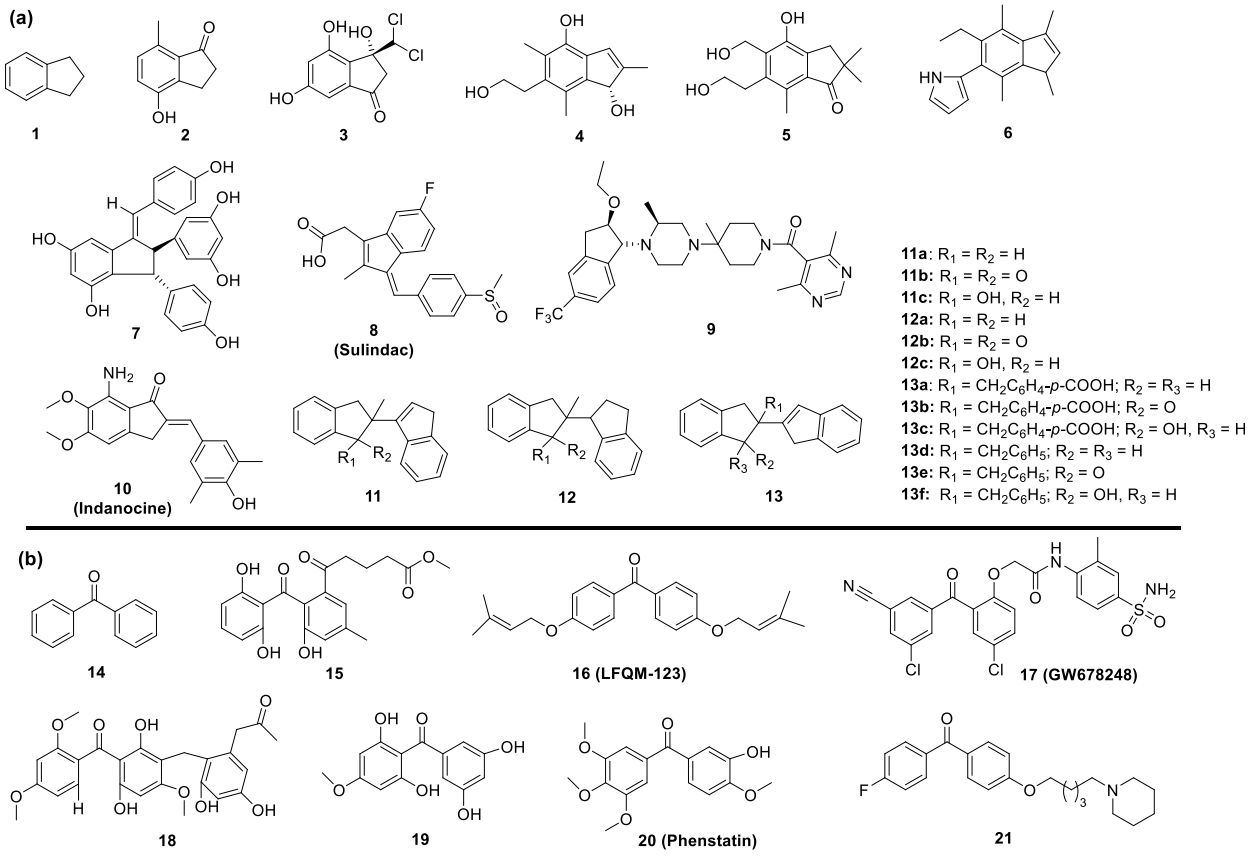

Fig. 1. Chemical structures of the indane core scaffold (1), examples of naturally occurring and synthetic indanes (2-13) (a) and benzophenones (14-21) (b) molecules under clinical use/investigation.

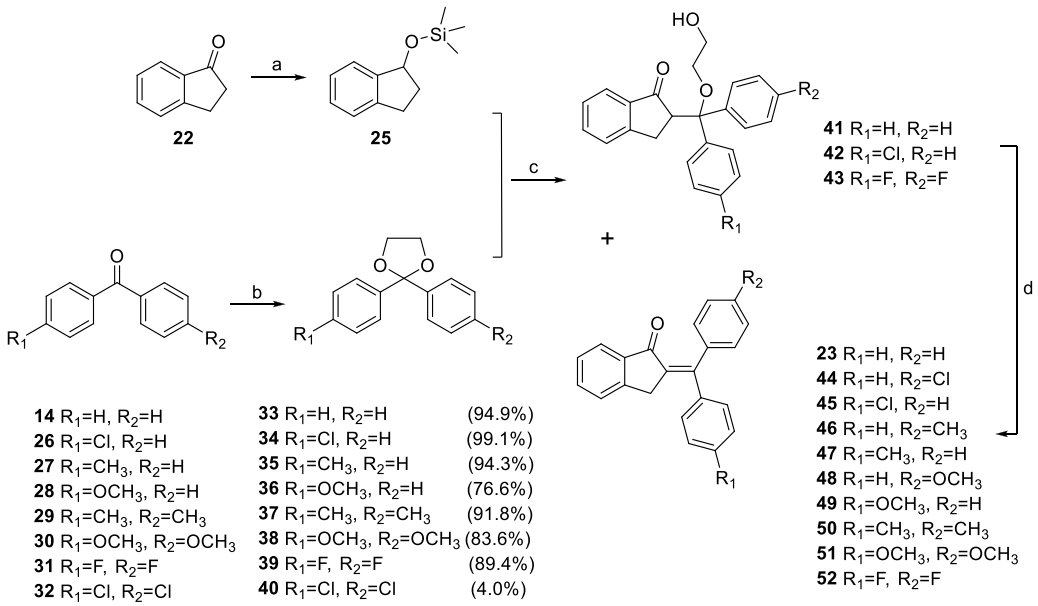

Scheme 1. Synthesis of new hybrid compounds (23), (44) – (52). Reagents and conditions: (a) triethylamine, trimethylsilyl trifluoromethanesulfonate (TMSOTf), dry dichloromethane (DCM), 0°C, N_2, 2 hrs, 75-90% yield; (b) ethylene glycol, trimethyl orthoformate (TMOF) and *p*-toluenesulfonic acid (PTSA), RT, 6- 21 days, 76.6-99.1% yield; (c) $SnCl_4$, dry DCM, -78°C, N_2, 1.5-3 hrs; (d) trifluoromethanesulfonic acid (TfOH), MeOH, DCM, reflux, 1-3 hrs.

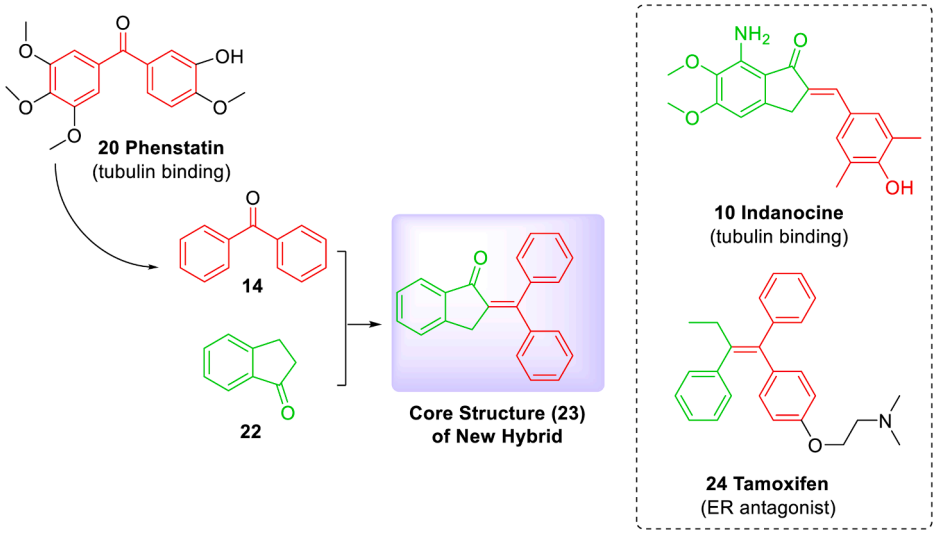

Fig. 2. Schematic representation of the novel indane-benzophenone hybrid 23 from the core structure of phenstatin (20) and 1-indanone (22) with potential anticancer activities by mimicking the structures of indanocine (10) and tamoxifen (24).

assigned relative to the middle $CDCl_3$ peak at 77.0 ppm. Chemical shifts (δ) are given in parts per million (ppm) and were referenced to solvent signals. Coupling constants are reported in Hertz. The number of scans was appropriate to generate good quality spectra for analysis. Both 1D and 2D NMR experiments were analysed with Bruker TopSpin 3.6.2 software. All HRMS data was obtained using a Thermo LTQ-Oribtrap Discovery mass spectrometer, and data analysis was performed using Xcalibre software. Mass measurement accuracies of $< \pm 5$ ppm were obtained. Crystallographic analyses of compounds were determined by X-ray Crystallography Facility'with Bruker SMART APEX or Rigaku Saturn-724 (2007). Crystallographic data for the structures in this paper have been deposited with the Cambridge Crystallographic Data Centre (CCDC) as supplementary publication: CCDC 2260975-2260977, Copies of the data can be obtained, free of charge, on application to CCDC, 12 Union Road, Cambridge CB2 1EZ, UK, [fax: +44-(0)1223-336033 or e-mail: deposit@ccdc.cam.ac.uk]. Uncorrected melting points (M.P.) were measured on a Gallenkamp apparatus. Details of the synthesis (general methods I, II and III) and characterisation of intermediate compounds, and NMR spectra of the compounds are available in the Supplementary Materials. The purity and stability of the compounds were analysed and confirmed by TLC before the compounds are used in the biological experiments.

2.1.1. General method IV for the aldol condensation of the hybrid alcohols

To a solution of appropriate alcohols (1 mol eq.) in MeOH/DCM (10 mL, 3:1, *v/v*) was added TfOH (1 mol eq.). The mixture was stirred under reflux for 1 - 3 hrs, after which time the reaction was quenched by addition of NaOH aqueous solution (2M, 20 mL), and the reaction mixture was extracted with DCM (3 × 25 mL). The combined organic extracts were concentrated *in vacuo,* and the residue was purified by flash column chromatography (hexane:EtOAc, 10:1). All homogeneous fractions were collected, and the solvent was removed *in vacuo* to afford

the desired enones.

2,3-dihydro-2-(diphenylmethylene)inden-1-one (23)

This was synthesised using the general method IV from the alcohol **41** to afford the product **23** as a yellow solid in 93% yield 93%; $R_f = 0.42$ (hexane:EtOAc, 5:1, *v/v*). M.P.: 62-68 °C. ^{1}H NMR ($CDCl_3$, 400 MHz) δ 3.89 (s, 2H, C$\underline{H}_2$), 7.31-7.46 (2 x m, 12H, Ar-$\underline{H}$), 7.59 (t, $J = 7.33$ Hz, 1H, Ar-$\underline{H}$), 7.83 (d, $J = 7.66$ Hz, 1H, Ar-$\underline{H}$). ^{13}C NMR ($CDCl_3$, 100 MHz) δ 33.69 ($\underline{C}H_2$), 123.85 ($\underline{C}H$), 125.37 ($\underline{C}H$), 126.97 ($\underline{C}H$), 127.49 (2 x $\underline{C}H$), 127.72 ($\underline{C}H$), 127.91 ($\underline{C}H$), 127.95 (2 x $\underline{C}H$), 128.68 (2 x $\underline{C}H$), 128.9 (2 x $\underline{C}H$), 132.45 (quat. $\underline{C}$), 133.77 ($\underline{C}H$), 139.36 (quat. $\underline{C}$), 139.39 (quat. $\underline{C}$), 141.61 (quat. $\underline{C}$), 148.44 (quat. $\underline{C}$), 150.59 (quat. $\underline{C}$), 192.39 ($\underline{C}$=O). HRMS: calculated for $C_{22}H_{16}O$ (296.1201); 230 found $(M+Na)^+$ *m/z* at 319.1112. (Figs. S23, S24 and S25 in the Supplementary Materials).

Enones **44** and **45** were synthesised using the general method IV from the alcohol **42** affording a 1:1 mixture of the desired isomers as yellow solid in 97% yield; $R_f = 0.54$ (**44**) and $R_f = 0.48$ (**45**) (hexane: EtOAc, 5:1, *v/v*).

(Z)-2-((4-chlorophenyl)(phenyl)methylene)-2,3-dihydro-1H-inden-1-one (44)

M.P.: 67-70 °C. ^{1}H NMR ($CDCl_3$, 400 MHz) δ 3.88 (s, 2H, C$\underline{H}_2$), 7.25 (d, $J = 8.08$ Hz, 2H, Ar-$\underline{H}$) 7.29-7.46 (m, 9H, Ar-$\underline{H}$), 7.60 (t, $J = 7.46$ Hz, 1H, Ar-$\underline{H}$), 7.82 (d, $J = 7.64$ Hz, 1H, Ar-$\underline{H}$); ^{13}C NMR ($CDCl_3$, 100 MHz) δ 33.66 ($\underline{C}H_2$), 123.88 ($\underline{C}H$), 125.39 ($\underline{C}H$), 127.07 ($\underline{C}H$), 127.74 (2 x $\underline{C}H$), 128.06 (2 x $\underline{C}H$), 128.13 ($\underline{C}H$), 128.69 (2 x $\underline{C}H$), 130.42 (2 x $\underline{C}H$), 132.90 (quat. $\underline{C}$), 133.72 (quat. $\underline{C}$), 133.96 ($\underline{C}H$), 137.73 (quat. $\underline{C}$), 139.18 (quat. $\underline{C}$), 141.15 (quat. $\underline{C}$), 148.40 (quat. $\underline{C}$), 149.11 (quat. $\underline{C}$), 192.35 ($\underline{C}$=O). HRMS: calculated for $C_{22}H_{15}ClO$ (330.0811); found: $(M+Na)^+$ *m/z* at 353.0715. (Figs. S26, S27 and S28).

(*E*)-2-((3-chlorophenyl)(phenyl)methylene)-2,3-dihydroinden-1-one (45)

M.P.: 67-70 °C. ^{1}H NMR ($CDCl_3$, 400 MHz) δ 3.87 (s, 2H, C$\underline{H}_2$), 7.26-7.29 (m, 4H, Ar-$\underline{H}$), 7.39-7.47 (m, 7H, Ar-$\underline{H}$), 7.60 (t, $J = 7.42$ Hz, 1H, Ar-$\underline{H}$), 7.81 (d, $J = 7.60$ Hz, 1H, Ar-$\underline{H}$). ^{13}C NMR ($CDCl_3$, 100 MHz) δ 33.64 ($\underline{C}H_2$), 123.90 ($\underline{C}H$), 125.37 ($\underline{C}H$), 127.08 ($\underline{C}H$), 127.59 (2 x $\underline{C}H$), 127.91 ($\underline{C}H$), 128.23 (2 x $\underline{C}H$), 128.87 (2 x $\underline{C}H$), 130.12 (2 x $\underline{C}H$), 132.80 (quat. $\underline{C}$), 133.90 ($\underline{C}H$), 133.96 (quat. $\underline{C}$), 138.94 (quat. $\underline{C}$), 139.22 (quat. $\underline{C}$), 139.95 (quat. $\underline{C}$), 148.21 (quat. $\underline{C}$), 149.15 (quat. $\underline{C}$), 192.17 ($\underline{C}$=O). MS: calculated for $C_{22}H_{15}ClO$ (330.0811); found: $(M+H)^+$ *m/z* at 331.0870. (Figs. S29, S30 and S31).

Enones **46** and **47** were synthesised using the general method III from the cyclic ketal **35** affording a 1:1 mixture of the desired isomers as yellow oils in 58% yield; $R_f = 0.53$ (**46**) and $R_f = 0.55$ (**47**) (hexane: EtOAc, 5:1, *v/v*).

(Z)-2-(phenyl(p-tolyl)methylene)-2,3-dihydro-1H-inden-1-one (46)

^{1}H NMR ($CDCl_3$, 400MHz) δ 2.41 (s, 3H, CH_3), 3.86 & 3.91 [2 x s (one major & one minor), 2H, C$\underline{H}_2$], 7.20-7.44 (m, 11H, Ar-$\underline{H}$), 7.58 (t, $J = 7.12$ Hz, 1H, Ar-$\underline{H}$), 7.82 (d, $J = 7.5$ Hz, 1H, Ar-$\underline{H}$). ^{13}C NMR ($CDCl_3$, 100MHz) δ (ppm): 21.01 ($\underline{C}H_3$), 33.78 ($\underline{C}H_2$), 123.83 ($\underline{C}H$), 125.30 ($\underline{C}H$), 126.91 ($\underline{C}H$), 127.81 ($\underline{C}H$), 127.89 (2 x $\underline{C}H$), 128.18 (2 x $\underline{C}H$), 128.70 (2 x $\underline{C}H$), 128.98 (2 x $\underline{C}H$), 132.13 (quat. $\underline{C}$), 133.64 ($\underline{C}H$), 136.34 (quat. $\underline{C}$), 137.72 (quat. $\underline{C}$), 139.50 (quat. $\underline{C}$), 141.87 (quat. $\underline{C}$), 148.37 (quat. $\underline{C}$), 150.91 (quat. $\underline{C}$), 192.38 ($\underline{C}$=O). HRMS: calculated for $C_{23}H_{18}O$ (310.1358); found: $(M+Na)^+$ *m/z* at 333.1261. (Figs. S32, S33 and S34).

(E)-2-(phenyl(p-tolyl)methylene)-2,3-dihydro-1H-inden-1-one (47)

^{1}H NMR ($CDCl_3$, 400MHz) δ 2.42 (s, 3H, C$\underline{H}_3$), 3.86 & 3.91 [2 x s (one minor & one major), 2H, C$\underline{H}_2$], 7.20-7.46 (3 x m, 11H, Ar-$\underline{H}$), 7.58 (t, $J = 7.35$ Hz, 1H, Ar-$\underline{H}$), 7.81 (d, $J = 7.35$ Hz, 1H, Ar-$\underline{H}$). ^{13}C NMR ($CDCl_3$, 100MHz) δ (ppm): 20.89 ($\underline{C}H_3$), 33.78 ($\underline{C}H_2$), 123.82 ($\underline{C}H$), 125.30 ($\underline{C}H$), 126.91 ($\underline{C}H$), 127.45 (2 x $\underline{C}H$), 127.60 ($\underline{C}H$), 128.60 (2 x $\underline{C}H$), 128.80 (2 x $\underline{C}H$), 128.87 (2 x $\underline{C}H$), 132.07 (quat. $\underline{C}$), 133.63 ($\underline{C}H$), 138.01 (quat. $\underline{C}$), 138.68 (quat. $\underline{C}$), 139.41 (quat. $\underline{C}$), 139.64 (quat. $\underline{C}$), 148.45 (quat. $\underline{C}$), 150.66 (quat. $\underline{C}$), 192.41 ($\underline{C}$=O). HRMS: calculated for $C_{23}H_{18}O$ (310.1358); found: $(M+Na)^+$ *m/z* at 333.1254. (Figs. S35, S36 and S37).

Enones **48** & **49** were synthesised and isolated using the general method III from the ketal **36** affording a 1:1 mixture of the desired isomers **48** and **49** as yellow oils in 18% yield; $R_f = 0.38$ (**48**), $R_f = 0.36$ (**49**) (hexane:EtOAc, 5:1, *v/v*); an uncharacterised product as white oil in 11% yield; $R_f = 0.17$ (hexane:EtOAc, 5:1, *v/v*).

(Z)-2-((4-fluorophenyl)(phenyl)methylene)-2,3-dihydro-*1H*-inden-1-one (48)

^{1}H NMR ($CDCl_3$, 400MHz) δ 3.83, 3.87 & 3.92 (3 x s, 5H, O$\underline{C}H_3$ & C$\underline{H}_2$), 6.92 (d, $J = 8.87$ Hz, 2H, Ar-$\underline{H}$), 7.28-7.34 (m, 4H, Ar-$\underline{H}$), 7.38-7.60 (3 x m, 10H, Ar-$\underline{H}$), 7.78-7.85 (m, 1H, Ar-$\underline{H}$). ^{13}C NMR ($CDCl_3$, 100MHz) δ 33.98 ($\underline{C}H_2$), 54.78 (O$\underline{C}H_3$), 112.71 (2 x $\underline{C}H$), 123.80 ($\underline{C}H$), 125.29 ($\underline{C}H$), 126.90 ($\underline{C}H$), 127.82($\underline{C}H$), 127.90 (2 x $\underline{C}H$), 128.82 (2 x $\underline{C}H$), 130.98 (2 x $\underline{C}H$), 131.26 (quat. $\underline{C}$), 131.59 (quat. $\underline{C}$), 133.61 ($\underline{C}H$), 139.65 (quat. $\underline{C}$), 142.16 (quat. $\underline{C}$), 148.33 (quat. $\underline{C}$), 150.93 (quat. $\underline{C}$), 159.42 (quat. $\underline{C}$), 192.36 ($\underline{C}$=O). HRMS: calculated for $C_{23}H_{18}O_2$ (326.1307); found: $(M+Na)^+$ *m/z* at 349.1212. (Figs. S38, S39 and S40).

(E)-2-((4-fluorophenyl)(phenyl)methylene)-2,3-dihydro-*1H*-inden-1-one (49)

^{1}H NMR ($CDCl_3$, 400MHz) δ 3.87 (s, 3H, O$\underline{C}H_3$), 3.95 (s, 2H, C$\underline{H}_2$), 6.94 (d, $J = 8.56$ Hz, 2H, Ar-$\underline{H}$), 7.28-7.42 (2 x m, 8H, Ar-$\underline{H}$), 7.47 (d, $J = 7.67$ Hz, 1H, Ar-$\underline{H}$), 7.59 (t, $J = 7.06$ Hz, 1H, Ar-$\underline{H}$), 7.81 (d, $J = 7.67$ Hz, 1H, Ar-$\underline{H}$). ^{13}C NMR ($CDCl_3$, 100MHz) δ (ppm): 33.94 ($\underline{C}H_2$), 54.89 (O$\underline{C}H_3$), 113.23 (2 x $\underline{C}H$), 123.79 ($\underline{C}H$), 125.29 ($\underline{C}H$), 126.91 ($\underline{C}H$), 127.50 (2 x $\underline{C}H$), 127.58 ($\underline{C}H$), 128.94 (2 x $\underline{C}H$), 130.67 (2 x $\underline{C}H$), 131.62 (quat. $\underline{C}$), 133.56 ($\underline{C}H$), 133.76 (quat. $\underline{C}$), 139.43 (quat. $\underline{C}$), 139.91 (quat. $\underline{C}$), 148.45 (quat. $\underline{C}$), 150.26 (quat. $\underline{C}$), 159.31 (quat. $\underline{C}$), 192.46 ($\underline{C}$=O). HRMS: calculated for $C_{23}H_{18}O_2$ (326.1307); found: $(M+H)^+$ *m/z* at 327.1408. (Figs. S41, S42 and S43).

2-(di-p-tolylmethylene)-2,3-dihydro-1H-inden-1-one (50)

Enone **50** was synthesised and isolated as yellow oil using the general method III from the ketal **37** in 42% yield, $R_f = 0.28$ (**50**) (hexane: EtOAc, 8:1, *v/v*). ^{1}H NMR ($CDCl_3$, 400MHz) δ 2.42 (s, 6H, 2 x C$\underline{H}_3$), 3.89 (s, 2H, C$\underline{H}_2$), 7.20 & 7.23 (2 x s, 8H, Ar-$\underline{H}$), 7.40-7.45 (m, 2H, Ar-$\underline{H}$), 7.58 (t, $J = 7.57$ Hz, 1H, Ar-$\underline{H}$), 7.82 (d, $J = 7.60$ Hz, 1H, Ar-$\underline{H}$). ^{13}C NMR ($CDCl_3$, 100MHz) δ 20.91 ($\underline{C}H_3$), 21.03 ($\underline{C}H_3$), 33.90 ($\underline{C}H_2$), 123.80 ($\underline{C}H$), 125.29 ($\underline{C}H$), 126.87 ($\underline{C}H$), 128.18 (2 x $\underline{C}H$), 128.57 (2 x $\underline{C}H$), 128.88 (2 x $\underline{C}H$), 129.01 (2 x $\underline{C}H$), 131.80 (quat. $\underline{C}$), 133.56 ($\underline{C}H$), 136.63 (quat. $\underline{C}$), 137.62 (quat. $\underline{C}$), 137.94 (quat. $\underline{C}$), 138.95 (quat. $\underline{C}$), 139.56 (quat. $\underline{C}$), 148.43 (quat. $\underline{C}$), 151.00 (quat. $\underline{C}$), 192.45 ($\underline{C}$=O). MS: calculated for $C_{24}H_{20}O$ (324.1514); found: $(M+Na)^+$ *m/z* at 347.1433. (Figs. S44, S45 and S46).

2-(bis(4-methoxyphenyl)methylene)-2,3-dihydro-*1H*-inden-1-one (51)

Enone **51** was synthesised and isolated using the general method III from the ketal **38** affording compound **51** as yellow oil in 17% yield; $R_f = 0.34$ (hexane:EtOAc:DCM, 8:1:1, *v/v/v*). ^{1}H NMR ($CDCl_3$, 400MHz) δ 3.87 & 3.89 (2 x s, 8H, 2 x O$\underline{C}H_3$ & C$\underline{H}_2$), 6.93 (t, $J = 10.02$ Hz, 4H, Ar-$\underline{H}$), 7.23-7.29 (m, 4H, Ar-$\underline{H}$), 7.38-7.45 (m, 2H, Ar-$\underline{H}$), 7.55-7.59 (m, 1H, Ar-$\underline{H}$), 7.82 (d, $J = 7.52$ Hz, 1H, Ar-$\underline{H}$). ^{13}C NMR ($CDCl_3$, 100MHz) δ (ppm): 34.17 ($\underline{C}H_2$), 54.77 (O$\underline{C}H_3$), 54.88 (O$\underline{C}H_3$), 112.73 (2 x $\underline{C}H$), 113.16 (2 x $\underline{C}H$), 123.75 ($\underline{C}H$), 125.21 ($\underline{C}H$), 126.83 ($\underline{C}H$), 130.76 (2 x $\underline{C}H$), 130.98 (2 x $\underline{C}H$), 131.79 (quat. $\underline{C}$), 133.42 ($\underline{C}H$), 134.34 (quat. $\underline{C}$), 139.72 (quat. $\underline{C}$), 148.36 (quat. $\underline{C}$), 150.67 (quat. $\underline{C}$), 159.25 (quat. $\underline{C}$), 159.34 (quat. $\underline{C}$), 192.44 ($\underline{C}$=O). HRMS: calculated for $C_{24}H_{20}O_3$ (356.1412); found: $(M+H)^+$ *m/z* at 357.1516. (Figs. S47, S48 and S49).

2-(bis(4-fluorophenyl)methylene)-2,3-dihydro-1H-inden-1-one (52)

Enone **52** was synthesised and isolated as yellow oil using the general method IV from the alcohol **43** in 87%; $R_f = 0.69$ (hexane:EtOAc, 5:1, *v/v*). ^{1}H NMR ($CDCl_3$, 400MHz) δ 3.87 (s, 2H, C$\underline{H}_2$), 7.07-7.15 (m, 4H, Ar-$\underline{H}$), 7.25-7.32 (m, 4H, Ar-$\underline{H}$), 7.40-7.47 (m, 2H, Ar-$\underline{H}$), 7.61 (td, $J_1 = 1.26$ Hz, $J_2 = 7.34$ Hz, 1H, Ar-$\underline{H}$), 7.82 (d, $J = 7.71$ Hz, 1H, Ar-$\underline{H}$). ^{13}C NMR ($CDCl_3$, 100MHz) δ (ppm): 34.22 ($\underline{C}H_2$), 114.94 ($\underline{C}H$), 115.16 ($\underline{C}H$), 115.47 ($\underline{C}H$), 115.68 ($\underline{C}H$), 124.34 ($\underline{C}H$), 125.83 ($\underline{C}H$), 127.58 ($\underline{C}H$), 131.15 ($\underline{C}H$), 131.23 ($\underline{C}H$), 131.39 ($\underline{C}H$), 131.47 ($\underline{C}H$), 133.24 (quat. $\underline{C}$), 134.43 ($\underline{C}H$), 135.43 & 135.46 (quat. $\underline{C}$), 137.84 & 137.88 (quat. $\underline{C}$),

139.66 (quat. C), 148.70 (quat. C), 148.76 (quat. C), 161.40 & 161.56 (quat. C), 163.88 & 164.03 (quat. C), 192.26 (C=O). HRMS: calculated for $C_{22}H_{14}F_2O$ (332.1013); found: $(M+H)^+$ *m/z* at 333.1089. (Figs. S50, S51 and S52).

2.2. X-Ray Crystallography

The data for the structure all structures were collected on a Rigaku Saturn 724 CCD Diffractometer. A suitable crystal was selected and mounted using inert oil on a 0.3 mm diameter glass fibre tip and placed on the goniometer head in a 108 K or 150 K N_2 gas stream. Data were collected and data integration, reduction and correction for absorption and polarization effects was performed using Crystallear-SM 1.4.0 software (Rigaku, 2006). Space group determination, structure solution and refinement were obtained using the SHELX software suite (XPREP (Bruker, 2014), XS (Sheldrick, 2008), XL (Sheldrick, 2015)). The structure was solved with Direct Methods using XS and refined against $|F^2|$ with the program XL using all data. Non-hydrogen atoms were refined with anisotropic thermal parameters. Hydrogen atoms were assigned to calculated positions using a riding model with appropriately fixed isotropic thermal parameters. Molecular graphics were generated using OLEX2 (Dolomanov et al., 2009). Crystal data, details of data collection and refinement are given in Tables S1 in the Supplementary Materials. Crystallographic data for the structure of compound **23** in this paper was published previously (Zhang et al., 2013); **23** was redetermined structurally to verify the geometry [x, x1] when a new batch crystal sample was obtained and the data has been deposited with the Cambridge Crystallographic Data Centre (deposition number: 1000642) (Zhang et al., 2014).

2.3. Biology

2.3.1. Cell culture

All cell lines were maintained in a humid chamber at 37 °C and 5% CO_2 atmosphere. SKBR3 (ATCC HTB-30™; human breast adenocarcinoma cells), MCF7 (ATCC HTB-22™; breast adenocarcinoma cells). While the growth of SKBR3 is oestrogen independent and the cells don't express oestrogen receptors, MCF7 are highly reliant on oestrogen for their growth, thus they highly express oestrogen receptors (Thompson et al., 1988). Another difference is that SKBR3 mimic "basal-like breast cancer" while MCF7 cells act as "luminal-like breast cancer" (Sharaf et al., 2022). The molecular characteristics of the four cancerous cell lines are shown in Tables S6 in the Supplementary Materials. MCF7 cells have been used due to the expression of ER and PR, and low levels of HER2. SKBR3, on the other hand, is a HER2+ cell line. Some authors have used this cell line due to the low expression of ER and PR (Aryapour et al., 2022; Dressing et al., 2012; Hevir et al., 2011; Holliday and Speirs, 2011, Muller et al., 2020). Weißenborn et al. (2014) have investigated the role of membrane-bound oestrogen receptor (GPER) as a potential tumour suppressor in MCF7 and SKBR3 breast cancer cells. GPER-specific agonist G-1 led to an inhibitory effect on MCF7 and SKBR3 breast cancer cells *via* induction of the cell cycle arrest and cell apoptosis. Moreover, GPER expression is regulated by epigenetic mechanisms. Our results propose that GPER may act as a potential therapeutic target once the cell surface expression of GPER makes it an excellent potential therapeutic target for non-triple-negative breast cancer. DU145 (ATCC HTB-81™; prostate carcinoma cells) were cultured in RPMI-1640 medium (Sigma-Aldrich) containing 10% fetal bovine serum (FBS) and 1% L-glutamine (Sigma-Aldrich). A549 (CCL-185™; lung carcinoma cells) was grown in Dulbecco's Modified Eagle's Medium F-12 Ham (Sigma-Aldrich) supplemented with 5% FBS and HEK-293 (ATCC CRL-1573™; embryonic kidney cells) was grown in Minimum Essential Medium Eagle (Sigma-Aldrich) supplemented with 10 % FBS.

2.3.2. Cytotoxicity assays

Cell cytotoxicity assays for chemical compounds were performed on DU145, A549, SKBR3, MCF7 and HEK-293 cell lines using the acid phosphatase (*p*-nitrophenyl phosphate) assay to determine their IC_{50}. In brief, DU145 and A549 cells were seeded in triplicate at equal densities (0.5×10^3 cells/well), SKBR3 and MCF7 at 1×10^4 cells/well and HEK-293 seeded at 2.5×10^4 cells/well, in 96 well culture plates. After 24 hrs, the cells were treated with a range of drug concentrations totalling a final volume of 200 μL/well. After 120 hrs, cell viability was achieved evaluating the cytosolic acid phosphatase as previously described by Marin & Clynes. (Martin and Clynes, 1993)

2.3.3. Cell viability - acid phosphatase assay

After 5 days of incubation of cells with the drugs, the medium was removed, and each well was washed with 100 μL of phosphate buffer solution (PBS). 100 μL of freshly prepared phosphatase substrate (10 mM *p*-nitrophenyl phosphate, Sigma-Aldrich) in 0.1 M sodium acetate (Sigma Ireland), 0.1 % Triton X-100 (BDH), pH 5.5, was then added to each well. The plates were wrapped in tinfoil and incubated in the dark at 37 °C 5% CO_2 for an hour. The reaction was terminated by the addition of 50 μL/well of NaOH (1 M) to cause an electrophilic shift in the *p*-nitrophenol chromofore and thus develop the yellow colour, which was measured in a dual beam plate reader at 405 nm with a reference wavelength of 620 nm. (Martin and Clynes, 1993)

2.3.4. Cell cycle analysis

Cell cycle was determined with SKBR3 breast cancer cells using propidium iodide (BD Pharmingen, Cat. No. 550474). DNA content was analysed by flow cytometry using BD Accuri C6 flow cytometer. The excitation wavelength was 488 nm and emission at 585 nm with bandwidth of 40 nm. A minimum of 3,000 cells per sample were analysed. Briefly, 6×10^4 cells/well were seeded in 24-well plate, and serum starved (1% FBS) for 24 hrs in incubator (37 °C, humidified atmosphere and 5% CO_2) to synchronise the cell cycle. Cells were exposed to different treatments (total 0.6 mL/well) in a range of concentration and incubated for 24, 72 and 120 hrs. Triplicates were obtained at 72 hrs. The cells were then harvested and washed with 1 mL of cold PBS. Cells were fixed using 1 mL of cold 70% ethanol added dropwise to ensure fixation of cells and minimise clumping, being then left at least 30 minutes on ice. This step is crucial once most of fluorescent DNA dyes are not membrane permeable. Cells were washed twice with PBS and centrifuged at higher centrifugal speed to pellet compared to unfixed cells (400 *g* for 5 mins). To ensure that only DNA is stained, cell pellet was treated with 50 μL of Ribonuclease A (100 μg/mL in PBS) to remove RNA, that would distort the results. Therefore, 300 μL of propidium iodide solution (50 μg/mL in PBS) was added directly to cells in RNAse A solution, mixed well and incubated in dark for 15 mins at 25 °C. The cell cycle distribution of 10,000 cells was recorded and the percentage of cells at G0/G1, S, and G2/M phases was analysed using FlowJo software. Debris and doublets were excluded from the analysis, which considered only single cells (BD Biosciences, Cell cycle Protocol).

2.4. Statistical analysis

The IC_{50} values were obtained from a non-linear regression fit curve of concentration log versus normalised response. Results were displayed as mean (n=3) ± Standard Error of the Mean (SEM) unless otherwise stated. Analyses were performed with the software GraphPad Prism® version 5.01. *P* values were obtained using One- and Two-way analyses of variance (Tzanova et al., 2009), and $p < 0.05$ was considered to be statistically significant.

3. Results and discussion

3.1. Chemistry

The preparation of the hybrid compounds is shown in Scheme 1 starting with the simple indanone structure and bore simplified substitution on the benzophenone derived portion of the scaffold, through the key step of direct aldol condensation. In the cross coupled aldol reaction, the presence of an enolisable ketone **25** is critical. In the current reaction sequence, the 1-indanone (**22**) portion of the hybrid was activated using a trimethylsilyl moiety, which converts the enol into a nucleophile leading to silyl enol ether **25** with 75-90% yield. Since the silyl enolate is moderately unstable, it was used directly after quenching, work-up and evaporation without purification by chromatography (Scheme 1-a).

The use of cyclic ketals in the protection of benzophenones is well established. (Erhan, 2008; Lukács et al., 2008; Lukács et al., 2004) The preparation of cyclic ketals (**33 - 40**) involved stirring the benzophenone with ethylene glycol, trimethyl orthoformate (TMOF) and p-toluenesulfonic acid (PTSA) at room temperature (RT) which afforded a high yield of product formation ranging from 76.6% to 99.1%, but over a prolonged reaction period from 4 to 21 days. The synthesis of compound **40** proved tedious with only 4% yield after 7 days; as a result, this compound wasn't investigated further (Scheme 1-b). However, further method development for this step is necessary.

The target α,β-unsaturated carbonyl hybrid enones (**23** and **44 - 52**) were obtained by condensation of the appropriate ketals (**33 - 40**) and the silyl enol-ether **25** catalysed by Lewis acid, tin(IV) chloride ($SnCl_4$), under dry conditions in dichloromethane (DCM) (Scheme 1-c). In the case of ketals **33** and **34**, the intermediate alcohols **41** (35%) and **42** (37%) were generated while generating significant quantities of the desired condensed hybrids **23** (21%) and **44/45** as isomeric mixture (26.0%) at the same time, respectively. For the *p*-difluoro derivative **39**, only the alcohol **43** (57%) was obtained without formation of enone **52** (Table S1 in the Supplementary Materials). The structures of alcohols **41** to **43** were confirmed from the ^{1}H Nuclear Magnetic Resonance (NMR) spectra based on the presence of three methylene groups and one methine group at the aliphatic region (as complex multiplets at δ 3.0-4.2 ppm, and one carbonyl group around δ 200 ppm in the ^{13}C NMR spectra (Figs. S17-S22 in the Supplementary Materials). Alcohols **41, 42** and **43** were subsequently dehydrated to the corresponding enone products **23, 44/45** and **52** by addition of trifluoromethanesulfonic acid (TfOH) under reflux (Scheme 1-d). Good yields were achieved: 93% for enone **23**, 97% for the mono chloro-isomeric enones **44/45** and 87% for the difluoro-enone derivative **52**. In other cases of the ketals **35 - 38**, the final hybrid products **46 – 51** were formed directly (without formation of the alcohols) in moderate yields 58% for the *p*-monomethyl isomeric mixture **46/47** and 42% for the *p*-dimethyl hybrid **50**, but poor yields for the isomeric mixture of **48/49** (18%) and 17% for the *p*-dimethoxy derivative **51** (Table S1).

The structures of the final desired hybrid molecules are confirmed by both NMR and high-resolution mass spectrometry (HRMS) experiments. The presence of one methene group (as a singlet at δ 3.89 ppm in the ^{1}H NMR spectrum), 14 methine groups, 6 x quaternary carbons at the aromatic region, and one carbonyl group (at δ 194 ppm in the ^{13}C NMR spectrum) were observed in compound **23**. The existence of one methyl group (being a singlet at δ 2.42 ppm in the ^{1}H NMR spectra in the case of **46** and **47**), one methoxy group (as a singlet at δ 3.95 ppm in the ^{1}H NMR spectra in the case of **48** and **49**), one methene group (as a singlet around δ 4.00 ppm in the ^{1}H NMR spectra), 13 methine groups, 7 x quaternary carbons at the aromatic region, and one carbonyl group (around δ 200 ppm in the ^{13}C NMR spectra) were observed for compounds **44 - 49**. In like manner, the *p*-dimethyl-hybrid **50** and the *p*-dimethoxy-hybrid **51** were also verified following the presence of two methyl groups as a singlet at δ 2.41 ppm, and two methoxy groups as a singlet at δ 3.87 ppm in the ^{1}H NMR spectra, respectively. The ^{1}H NMR spectrum of the *p*-monomethoxy derivative **51** showed 17 aromatic protons, one methoxy group (two peaks splitting at δ 3.66 and 3.67 ppm) and two methene groups (as two multiplets between δ 3.37 - 3.57 ppm) in the aliphatic region. In the ^{13}C NMR spectrum, it was observed two methene groups (δ 31.06 and 31.16 ppm), two aliphatic methine groups (δ 49.65 and 49.72 ppm), and one methoxy group (δ 54.62 ppm). The aliphatic quaternary carbon splits into two peaks: δ 55.87 and 56.5 ppm (higher intensity).

The isomeric mixtures (*Z*/*E*) of **44/45, 46/47** and **48/49** were separated by flash column chromatography. Crystallographic analysis was decisive in establishing the correct configuration of the isolated isomers: the *Z* stereochemistry of **44** and the *E* stereochemistry of **47** and **49**. The X-ray analysis also allowed the conclusion that the upper band on the thin layer chromatography (TLC) for the isomeric mixture of *p*-mononchloro **44** and *p*-monomethyl **47** hybrids was associated with the *Z* configuration and the first isomer eluted from the chromatography separation. Another characteristic observation was an inversion on the ^{13}C NMR spectra for the *Z* isomer: one methine group at δ 127.8 ppm, two methine groups at δ 127.89 ppm; for the *E* isomer: two methine groups at δ 127.45 ppm and one methine group at δ 127.6 ppm. However, an inversion in the elution pattern was observed in the same mobile phase system for the *p*-methoxy hybrid **49**, where the *E* configuration **49** being the upper band on the TLC and eluting from the column first.

The structures of compounds **23, 44, 47** and **49** are shown in Table 1 and Fig. S59. The crystal data and structure refinement are given in Table S2. Except for **47**, all molecules show one unique molecule in the asymmetric unit. Compound **47** has three separate unique molecules in the asymmetric unit. All molecules display the expected geometry around the central trigonal planar carbon with the exocyclic double bond to the indanone. The phenyl rings are twisted with respect to the plane of the indanone, and torsion angles from the exocyclic bond to the rings show the differences between molecules (see Table S3 and the overlay plot in Fig. S60). Some diphenylmethylidene substituted indanone compounds have been reported in the literature and show similar structural parameters. (Kumar et al., 2021; Zhou et al., 2019; Zhou, 2019)

The synthesis of phenstatin (**20**) followed Ghinet's procedure (Ghinet et al., 2011) starting with 2-methoxyphenol (**53**), but with some improvements. The acetate **54** was obtained by several recrystallisations (72% yield) instead of the single recrystallisation step reported. The TLC mobile phase system using ethyl acetate (EtOAc):toluene (6:1, *v:v*) was found to provide better separation than the reported EtOAc:heptane (6:4, *v:v*) (Scheme 2-a). Eaton's reagent was also prepared in-house from phosphorus pentoxide in methanesulfonic acid (1:10, *w:w*) (Scheme 2-b). It is important to note that the Eaton's reagent should be used at cold temperature based on the observation of deprotection of compound **54**. This wasn't reported in the original Ghinet protocol. The final step (Scheme 2-c) took an hour to go to completion yielding 97 % of phenstatin (**20**). The use of methanol (instead of ethanol reported) step was proved to be superior for the recrystallisation. The structures of **54, 55** and **20** were confirmed (Figs. S53-S58). The data was in an agreement with the literature values. (Ghinet et al., 2011; Wu et al., 2005)

3.2. Biology

3.2.1. Cytotoxicity analysis

The *in vitro* cytotoxicity evaluation was performed using the acid phosphatase assay (Martin and Clynes, 1993) against four cell lines: SKBR3 human breast cancer, MCF7 human breast cancer, A549 non-small cell lung cancer and DU145 prostate cancer, over a range of concentrations (0.004 μM to >100 μM). Antimitotic drugs, indanocine (**10**), phenstatin (**20**) and tamoxifen (**24**) were used as controls. The novel hybrid molecules targeted in this study are a combination of two fragments: 1-indanone and benzophenone fragments (Fig. 2). The cytotoxicity results of the two chemical fragments were evaluated first to establish whether the activity of the hybrid target scaffolds was

Table 1
Molecular structures of the final isolated hybrid compounds 23, 44, 47 and 49 with 50% thermal displacement. CCDC: The Cambridge Crystallographic Data Centre.

Compound	Structure	X-ray representation	Deposition Number (CCDC)
23	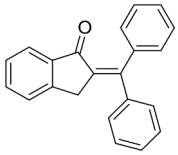	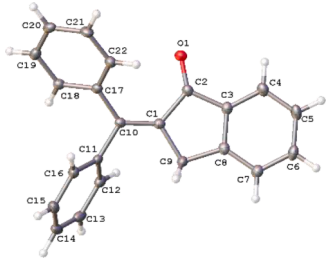	1000642
44	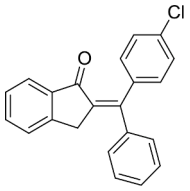	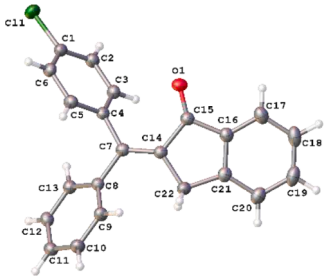	2260975
47	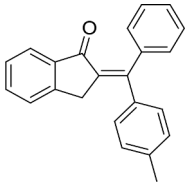	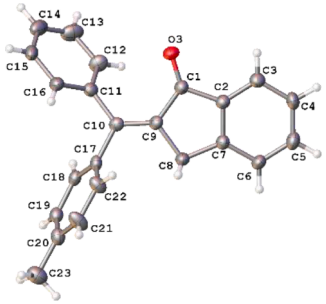	2260976
49	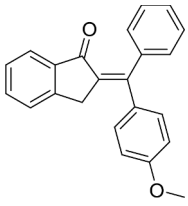	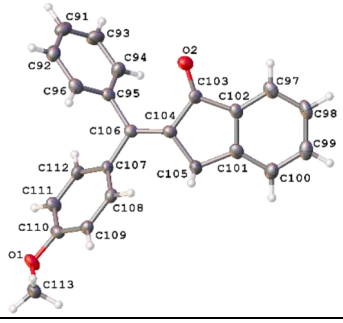	2260977

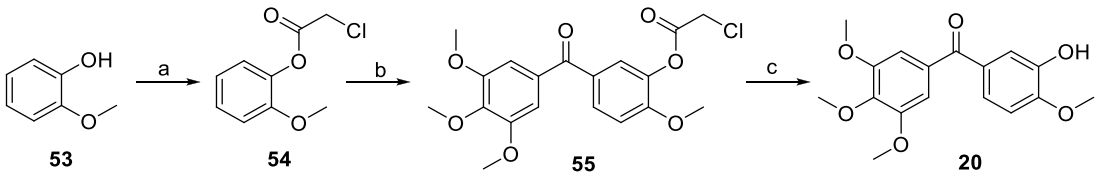

Scheme 2. Synthetic procedure of phenstatin (20). Reagents and conditions: (a) chloroacetyl chloride, 135°C, 8h, 72%; (b) 3,4,5-trimethoxybenzoic acid, Eaton's Reagent, 60°C, 4 h, 40%; (c) sodium acetate trihydrate, MeOH, reflux, 2 h, 97%.

significantly different than their constituent parts (Table 2). The greatest cytotoxic activities shown by the starting materials were against the prostate cancer cells (DU145) with IC_{50} values ranging from 31.4 μM (with monomethyl-substituted benzophenone **27**) to 46.3 μM (with dichloro-substituted benzophenone **32**). Compounds **20, 23, 24, 46** and **47** were selected and tested against the noncancerous Hek 293 cells. Similar to the effects of internal control tamoxifen (**24**) and phenstatin (**20**), the indicated compounds exhibited cytotoxic activity against both normal and cancerous cell lines (Table S5). The very wide variability in IC_{50} values for indanocine (**10**) and phenstatin (**20**) (Table 2) suggests the need for additional studies to increase the sample size.

In marked contrast, the cytotoxicity exhibited by **14, 22, 26 - 32** and **56** on HER2+ breast cancer cell line (SKBR3) and ER+ breast cancer cells (MCF7) was over 100 μM for all the compounds. All simple benzophenones were shown not be active against SKBR3 (Pettit et al., 2000) and MCF7 (ER+) cells. Phenstatin (**20**), the most substituted synthetic benzophenone, demonstrated a greater cytotoxicity in the nanomolar range [IC_{50} 0.004 μM (DU145) - 0.017 μM (A549), even for the two

Table 2
IC_{50} values of the chemical fragments, substituted benzylidenes, designed hybrids and controls against cancer cell lines SKBR3, MCF7, A549 and DU145. Results are expressed as Mean (SEM) of three independent experiments.

Compound	Cytotoxicity average IC_{50} μM (SEM)			
	SKBR3	MCF7	A549	DU145
10*	1.07 (0.096)	0.79 (0.14)	0.098 (0.12)	0.004 (0.13)
20*	0.51 (0.96)	0.035 (0.09)	0.017 (0.16)	0.004 (0.16)
24*	25.2 (0.14)	11.0 (0.55)	11.1 (0.22)	8.07 (0.20)
14#	> 100	> 100	> 100	37.6 (1.64)
22#	> 100	> 100	> 100	42.1 (1.7)
26#	> 100	> 100	> 100	37.1 (2.82)
27#	> 100	> 100	79.9 (1.24)	31.4 (3.70)
28#	> 100	> 100	67.1 (0.89)	36.8 (3.17)
29#	> 100	>100	50.4 (2.72)	33.6 (2.22)
30#	> 100	> 100	82.6 (3.90)	34.4 (5.05)
31#	> 100	> 100	> 100	39.6 (3.83)
32#	> 100	> 100	> 100	46.3 (3.24)
23+	58.6 (2.20)	~100.0	36.1 (2.50)	16.0 (1.31)
44+	32.7 (4.58)	38.8 (9.51)	24.9 (4.82)	22.5 (4.09)
45+	10.0 (1.01)	11.1 (1.03)	17.0 (4.88)	17.3 (0.12)
46+	27.3 (3.40)	37.2 (1.43)	22.83 (0.45)	29.9 (2.58)
47+	1.04 (0.35)	35.7 (1.34)	14.9 (0.42)	23.0 (2.61)
48+	22.01 (1.60)	34.59 (1.33)	15.0 (0.29)	27.83 (0.31)
49+	13.96 (0.70)	10.1 (0.71)	9.01 (0.45)	7.76 (0.26)
50++	9.72 (0.49)	32.8 (10.1)	35.6 (1.56)	62.4 (3.35)
51++	16.9 (2.14)	~100.0	28.5 (10.37)	28.1 (0.54)
52++	50.4 (0.63)	46.9 (0.98)	30.5 (5.41)	47.8 (3.83)
56^	~ 100	> 100	81.8 (2.00)	41.7 (1.96)
57^	11.61 (3.00)	52.0 (2.51)	28.31 (4.82)	23.96 (0.85)
58^	38.3 (0.76)	88.0 (2.64)	60.2 (0.56)	20.8 (0.52)
59^	42.0 (4.00)	60.6 (7.06)	49.2 (5.02)	16.6 (1.46)

* Controls: Indanocine (10); Phenstatin (20); Tamoxifen (24).
\# Starting materials: 1-indanone and benzophenones.
\+ Monosubstituted hybrids products.
++ Disubstituted hybrids products.
^ Monosubstituted benzylidenes.

breast cancer cell lines: 0.035 μM in MCF7 and 0.51 μM in SKBR3]. These results are well in agreement with the literature data of phenstatin (**20**): 0.034 μM (Barbosa et al., 2009) and 0.044 μM (Pettit et al., 2000) in MCF7 cells, and 0.003 μM in DU145 (Pettit et al., 2000). However, IC_{50} of 0.8 μM in MCF7 has been reported. (Kamal et al., 2015) For comparison, disubstituted 1-indanone **56** (Fig. 3) was included in the screening, and the incorporation of two methoxy groups on the aromatic ring didn't seem to change the cytotoxicity much toward the chosen cell lines, but **56** demonstrated increased cytotoxicity (IC_{50}: 81.8 μM) when compared to 1-indanone (**22**) (IC_{50} > 100 μM) in A549 cells.

Based on Table 2, both the internal controls: indanocine (**10**) and phenstatin (**20**) showed a remarkable selectivity against DU145 cells compared to other cell lines; however, tamoxifen (**24**) was non-selective. Not too far in comparison with tamoxifen, the hybrids 44, 45, 46, 48, 49, 50 and 52 presented a consistent cytotoxicity across the four cancer cell lines tested. Besides, compounds (**14, 22, 26-32**) provided a higher effect on prostatic cancerous DU145 cells compared to the other cancer cell types. In contrast, most monosubstituted hybrids products exhibited non-selectivity against cancerous cells except the unsubstituted molecule **23** and the *E*-methyl substituted molecule **47** which exerted more cytotoxic effect against DU145 and SKBR3, respectively. *p*-Methoxy-hybrids, *Z*-isomer **48** and *E*-isomer **49**, displayed a slightly more selective action against lung cancerous A549 cells than the other cell lines. Similar pattern was also observed with disubstituted hybrids products, where the *p*-dimethyl hybrid **50** and the *p*-dimethoxy hybrid **51** were slightly more selective against SKBR3 and compound **52** was rather more toxic on A549 than the rest cell lines. Monosubstituted benzylidenes **58** and **59** showed more selectivity to a certain extent towards the prostatic DU145 cells except compound **57** which had a clearer toxic potential on the breast SKBR3 cells compared to the other cell lines.

3.2.1.1. Cytotoxicity of mono-substituted hybrid molecules. The only information about 2,3-dihydro-1H-inden-1-one derivatives obtained from literature is related to their synthesis and X-ray crystallographic characterisation. (Ali et al., 2011; Asiri et al., 2012; Yang et al., 2012). Therefore, in this study it is the first time that the cytotoxicity for the novel hybrid indane scaffold is reported, but also the related mono- and poly-substituted benzylidenes (Table 2). Statistical analysis [One way ANOVA followed by Bonferroni's post hoc test represented as mean + SEM (n=3)] was used to compare the IC_{50} values of the hybrid products to their respective benzophenone molecules and indanone (**22**), a general increment on the cytotoxicity was achieved with substitution. The only exception observed was *Z*-methyl-substituted **46** which did not show a statistically significant lower cytotoxic activity on DU145 cells (29.9 μM) when compared with the IC_{50} of **22** being 42.1 μM and **27** being 31.4 μM.

This unsubstituted molecule **23** was the prototype of the new and targeted scaffold. It served as a primary guide for the synthetic route optimisation and for the bioactivity evaluation. Hybrid **23** demonstrated a significant increase ($p < 0.01$) in cytotoxicity against A549 cells when compared to its both starting materials **22** and **14**; a statistically significant increase in potency against breast cancer cells, SKBR3 ($p < 0.05$) and MCF7 ($p < 0.01$). In DU145 cells, **23** was statistically different than **22** ($p < 0.001$) and **14** ($p < 0.01$) (Table 2 & Fig. S61A in the Supplementary Materials).

The *E* configuration isomer **45** provided a higher potency than the *Z* isomer **44** across the chosen cancer cell lines, especially in SKBR3 cells: 10 μM of IC_{50} for **45** and 32.7 μM for **44**. Both molecules demonstrated a statistically significant increase in the cytotoxic activity ($p < 0.001$) compared to the parent molecules **22** and **26** on SKBR3 cells. Both isomers on A549 cells showed to be statistically significant compared to 1-indanone (**22**) ($p < 0.001$) and 4-chlorobenzophenone (**26**) ($p < 0.01$) but were slightly different in DU145 cells [**45** *vs* **22** ($p < 0.01$), **45** *vs* **26** ($p < 0.05$); **44** *vs* **22** ($p < 0.05$)]. Interestingly, closer potency was demonstrated for *Z* and *E* isomers against A549 (**44** with 24.9 μM; **45** with 17.0 μM) and DU145 (**44** with 22.5 μM; **45** with 17.3 μM) (Table 2

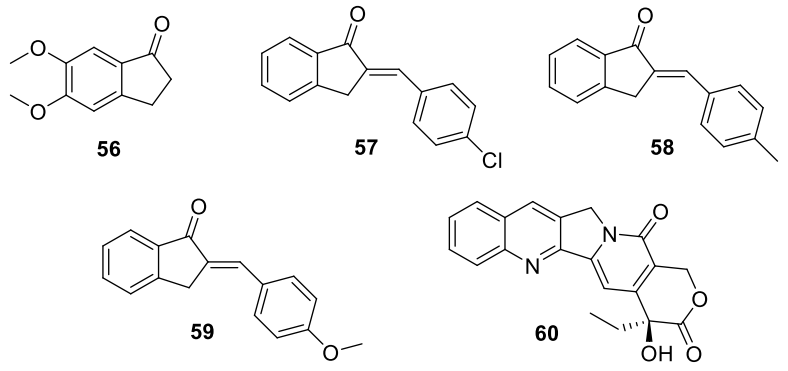

Fig. 3. Chemical structures of disubstituted 1-indanone 56 and monosubstituted benzylidenes 57, 58, 59 and camptothecin (60).

& Fig. S61B). Despite the significant difference between the IC_{50} values found for both *p*-chloro hybrids **44** and **45**, and their respective starting materials, there was no statistical difference between the cytotoxicity presented by both *Z* and *E* configurations on the four cell lines.

Similar pattern observed for the *p*-chloro hybrid molecules was also seen for *p*-methyl derivatives **46** and **47**, where increased cytotoxicity was observed with both hybrids compared to the parent molecules: 1-indanone (**22**) and 4-methyl-benzophenone (**27**). The *E* isomer **47** was statistically more cytotoxic when compared with the respective starting materials **22** and **27** on SKBR3 cells ($p < 0.01$) and A549 cells ($p < 0.001$). Isomer **47** demonstrated more than 20-fold higher potency (IC_{50} of 1.04 μM) on SKBR3 HER2+ breast cancer cell line than the *Z* isomer **46** (27.3 μM). However, no statistical significance was found when comparing *E* isomer **47** with its *Z* isomer **46**. On MCF7 cells, *Z* configuration **46** and *E* configuration **47** isomers were significantly more cytotoxic ($p < 0.001$) in comparison to **22.** In addition, **47** showed to be the most cytotoxic among all the hybrid molecules synthesised, with pronounced selectivity against SKBR3 cells (Table 2 & Fig. S62A). Overall, *E* configuration of the hybrid molecules **45** and **47** exhibited a higher cytotoxic potential against HER2+ breast cancer cell line SKBR3 than the Z configurations **44** and **46**, respectively or the parent molecules **22** and **27**.

Both *p*-methoxy hybrids *Z* isomer **48** and *E* isomer **49** showed a significant increase in cytotoxicity when compared with their parent fragments **22** and **28** against all four cell lines, especially for the *E* configuration. Hybrid **49** (IC_{50} of 7.76 μM) was significantly more cytotoxic ($p < 0.01$) toward the prostate cancer DU145 cell line than its *Z* isomer **48** (IC_{50} of 27.83 μM). However, no statistically significant difference was verified between the cytotoxicity values of **49** and **48** on SKBR3 (13.96 μM and 22.01 μM, respectively), MCF7 (10.1 μM and 34.59 μM, respectively) and A549 (9.01 μM and 15.0 μM, respectively) cell lines (Table 2 & Fig. S62B). Even though **49** exhibited low selectivity, its IC_{50} around 10 μM in these four cancer cell lines encourages further investigation into its mechanism of action.

When comparing with tamoxifen (**24**), the ER antagonist, tamoxifen exhibited the lowest potency (IC_{50}: 25.2 μM) against HER2+/neu breast cancer cells (SKBR3), while hybrid **47** was surprisingly selective (IC_{50}: 1.04 μM). Hybrid **49**, like tamoxifen, demonstrated consistent cytotoxicity over the four cell lines, however in SKBR3 cells **49** showed an IC_{50} nearly half of tamoxifen (**24**).

3.2.1.2. Cytotoxicity of monosubstituted benzylidenes. To explore structure-activity relationship further, commercially available benzylidene compounds: indanocine (**10**), *p*-chlorobenzylidene **57**, *p*-methyl-benzylidene **58** and *p*-methoxybenzylidene **59** (Fig. 3) were also screened for cytotoxic activity due to the structural similarity to the novel hybrid molecules envisioned in the study (Table 2).

The effects of an additional aromatic ring on the benzylidene scaffold are evident by results. For *E-p*-chloro-hybrid **45**, the addition of the second aromatic ring increased potency against MCF7 (5-fold, IC_{50}: 11.1 μM), A549 (1.7-fold, IC_{50}: 17.0 μM), and DU145 (1.4-fold, IC_{50}: 17.3 μM) cell lines when compared to its respective *p*-chloro-benzylidene **57**. There was no cytotoxicity difference between **57** (IC_{50}: 11.61 μM) and **45** (IC_{50}: 10.0 μM) towards SKBR3 cells. The results obtained on MCF7 cells showed a 2.5-fold increased cytotoxic potency (IC_{50}: 35.7 μM) for *E-p*-methyl-hybrid **47** compared to methyl-benzylidene **58** (IC_{50}: 88.0 μM); and 4-fold higher (IC_{50}: 14.9 μM) for **47** than **58** (IC_{50}: 60.2 μM) on A549 cancer cells. This difference became even more significant on SKBR3 where the cytotoxicity of hybrid **47** (IC_{50}: 1.04 μM) was 36.8-fold higher than methyl-benzylidene **58** (IC_{50}: 38.3 μM). *E-p*-methoxy-hybrid **49** exhibited a 3-fold higher cytotoxicity (IC_{50}: 13.96 μM) than methoxy-benzylidene **59** (IC_{50}: 42.0 μM)) on SKBR3 cells. When analysing the results obtained in MCF7 cells, hybrid **49** had 6-fold increased potency (IC_{50}: 10.1 μM) than methoxy-benzylidene **59** (IC_{50}: 60.6 μM), and 5-fold higher **49** (IC_{50}: 9.01 μM) than **61** (IC_{50}: 49.2 μM) against A549 cells. Taken together, the addition of the second benzyl ring to this novel indane scaffold of the *E* isomeric hybrids **47, 45** and **49** enhanced their cytotoxicity against the cancerous SKBR3 (HER2+), MCF7 (ER+), and A549 (NSCLC) cell lines, respectively.

3.2.1.3. Cytotoxicity of indanocine (). A short number of publications related to cytotoxicity of indanocine (**10**), a polysubstituted benzylidene, are available and most of these towards its anti-microtubule activity, exploring its potential on multidrug-resistant cells. No data so far has been found about the effects of indanocine on the chosen cell lines (SKBR3, MCF7, A549 and DU145) in this study and we report the results obtained for indanocine for the first time. On the other hand, this fact also limits a direct comparison between our results and those of from the literature. Therefore, a broader interpretation is necessary, and we evaluate our findings considering the type of cancer cell types we used and bioactive molecules structurally related to indanocine.

In a direct comparison with *E-p*-monomethyl-substituted hybrid **47**, Indanocine (**10**) exhibited an increased cytotoxicity 45-fold higher on MCF7 cells, 152-fold potent on A549 cells and reached 5,750-fold on DU145 cells. More interestingly, it presented nearly the same IC_{50} (1.07 μM) on SKBR3 cells as the hybrid **47** (IC_{50}: 1.04 μM).

3.2.1.4. Cytotoxicity of disubstituted benzylidenes. In SKBR3 cell line, the hybrids *p*-substituted dimethyl **50** and dimethoxy **51** substituents showed higher potency (IC_{50}: 9.72 μM and 16.9 μM, respectively) than the corresponding *Z-p*-methyl **46** (IC_{50}: 27.3 μM) and *Z-p*-methoxy **48** (IC_{50}: 22.01 μM) scaffolds (Table 2). No increase in the cytotoxicity was observed for all three hybrids **50, 51** and difluoro **52** on the prostate cancer cell line (DU145) when compared to the parent molecules: 1-indanone (**22**) and respective benzophenones (Fig. S63).

Comparing to the unsubstituted hybrid **23**, similar activity for these disubstituted molecules was seen on A549 lung cancer cells (Table 2). Interestingly, hybrid **23** (IC_{50}: 16.0 μM) showed higher potency on DU145 cells. Dimethyl hybrid **50** was the most cytotoxic in this group against SKBR3 (IC_{50}: 9.72 μM) and MCF7 (IC_{50}: 32.8 μM) cells. It was also verified that dimethyl hybrid **50** was less cytotoxic than the *p*-monomethyl substituted *Z* isomer **46** and *E* isomer **47** against A549 and DU145 cell lines (Table 2). The most significant difference was observed on SKBR3 cells where the presence of the methyl at *Z-p*-position to the carbonyl in **46** (IC_{50}: 27.3 μM) was responsible for the decrease of cytotoxicity compared to the dimethyl hybrid **50** (IC_{50}: 9.72 μM) (Fig. S64). Surprisingly, the absence of the methyl at *Z* position was responsible for the increase of the cytotoxic potency seen in *E* configuration hybrid **47** (IC_{50}: 1.04 μM). Following these results, methyl substituent at *E-p*-position **47** showed a selective cytotoxicity on SKBR3 cancer cells.

3.2.2. Cell cycle analysis

Superficially, the connection between the cell cycle and cancer is obvious: cell cycle machinery controls cell proliferation, and cancer is a disease of inappropriate cell proliferation. Fundamentally, all cancers permit the existence of too many cells (Collins et al., 1997). The ability to modulate the life or death of a cell is recognised for its immense therapeutic potential. Therefore, research continues to focus on the elucidation and analysis of the cell cycle machinery and signalling pathways that control cell cycle arrest and apoptosis (Elmore, 2007). Although toxicants may initiate cell damage or stress, the cellular proteins that are involved in control of the cell cycle and apoptosis are the final arbiters of cell fate (Pucci et al., 2000). In this study, ER/PR–-negative HER2+ breast cancer cells (SKBR3) were chosen taking in consideration their sensitivity to the lead hybrid molecule **47** as observed on the cytotoxicity assays. Flow cytometry histograms of propidium iodide stained cells treated for 24 hrs and 120 hrs with 10 μM of the respective compounds **23, 47** and **49** can be found in Fig. 4. Based on these results, an intermediate time-point (72 hrs) was chosen for the full analysis (Table 3). Indanocine (**10**), tamoxifen (**24**),

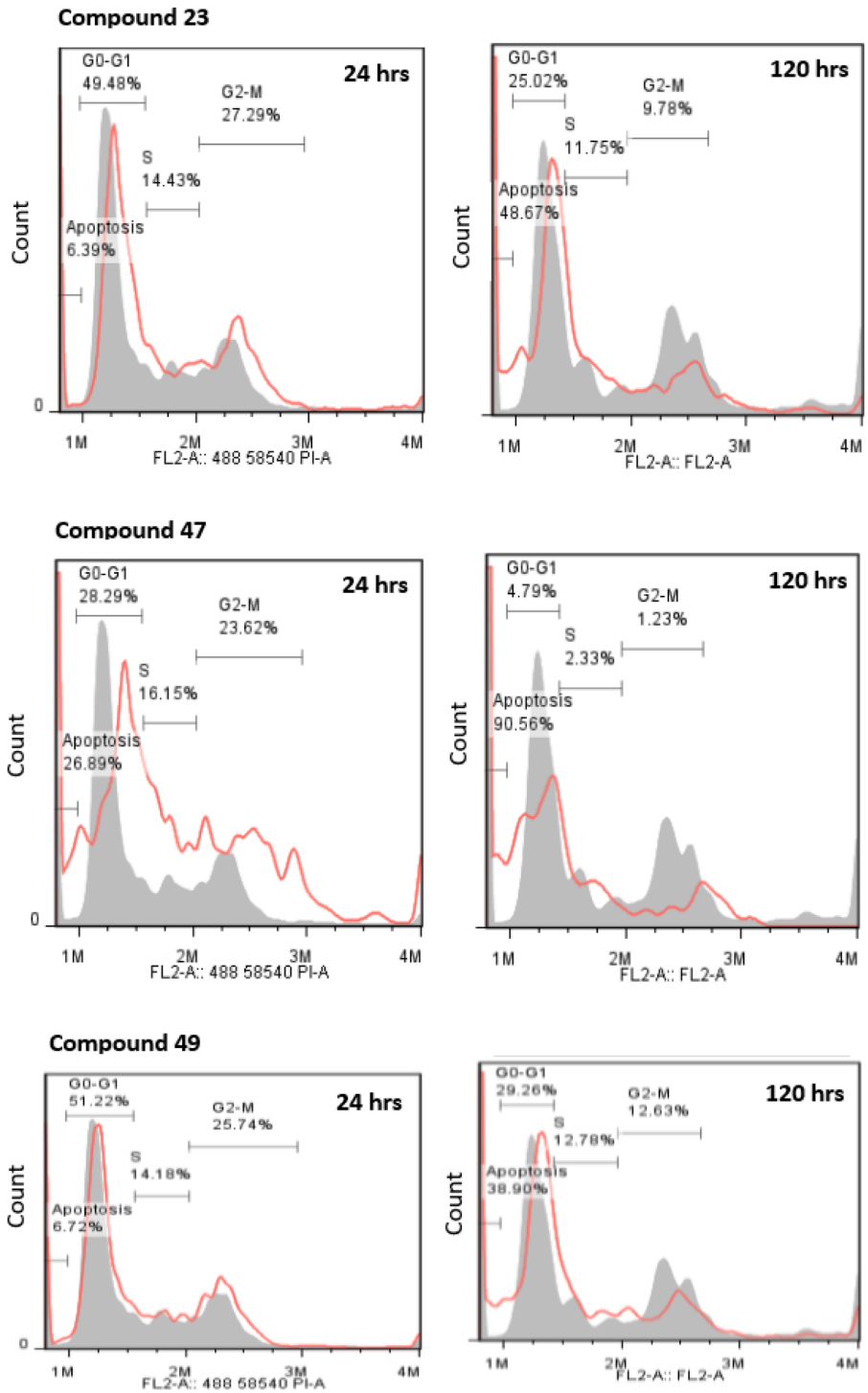

Fig. 4. DNA flow cytometry histograms of PI-stained SKBR3 cells treated with 10 μM of 23, 47 and 49 (red line) for 24 hrs and 120 hrs and compared to the untreated cells (grey background).

methyl-benzylidene (**58**), methoxy-benzylidene (**59**) and camptothecin (**60**) were used in different combinations as internal controls and the cell cycle on SKBR3 was evaluated along with the hybrid molecules (Fig. 4, Table 3 and Table S4).

3.2.2.5. Cell cycle effect of mono- and polysubstituted benzylidenes. Very few data were available in literature in relation to the bioactivities of indanocine (**10**), methyl- (**58**) and methoxy-(**59**) benzylidenes, especially in the case of cell cycle arrest on SKBR3 cells. Leoni and colleagues have tested indanocine in stationary-phase cell lines and have observed that up to 81% of stationary MCF7/ADR cells (one week in confluent culture) were in the G1 phase of the cell cycle (Leoni et al., 2000). The cytotoxic effect of indanocine in non-cycling MCF7/ADR cells has been confirmed by the detection of an apoptotic sub-G0/G1 population by flow cytometry and by the activation of caspase-3. Parental (wild type) MCF7 cells were similarly growth arrested but did not show apoptotic features. In our study, the treatment with 10 μM of **10, 58** and **59** for 24 hrs didn't affect cell cycle in SKBR3 (Table S4), but an increase in apoptosis was observed after 120 hrs treatment as reflected by the increase of cell population in sub-G1 phase. While methyl-benzylidene **58**

Table 3
Cell cycle analysis of 10,000 events using SKBR3 breast cancer cells treated for 72 hrs. Results are expressed as Mean ± (SEM) of 3 independent experiments. Two-way ANOVA and Bonferroni posttest were used. *($p < 0.05$), **($p < 0.01$), ***($p < 0.001$).

Compound	Conc. (μM)	Cell cycle distribution % (SEM)			
		Sub-G1	G0-G1	S	G2-M
Untreated	0	5.79 (1.11)	61.99 (2.81)	9.06 (1.01)	18.46 (1.16)
23	10	5.42 (0.79)	57.34* (4.46)	13.45 (2.0)	18.34 (0.83)
	30	7.26 (0.84)	53.37*** (3.37)	13.62* (1.20)	19.36 (0.6)
46	10	5.30 (0.48)	58.11 (2.01)	13.05 (0.46)	18.0 (0.94)
	30	7.53 (1.57)	53.36*** (2.49)	14.44* (1.69)	18.28 (0.48)
47	10	12.13** (0.24)	46.96*** (6.16)	18.5*** (4.78)	15.63 (0.67)
	30	20.36*** (2.6)	31.18*** (0.56)	25.83*** (1.4)	13.36* (0.64)
50	10	5.86 (0.54)	57.68 (2.97)	13.36 (0.85)	17.46 (0.78)
	30	8.2 (0.25)	45.80*** (2.17)	20.26*** (0.6)	17.20 (0.16)
24	10	6.46 (0.78)	62.49 (3.26)	9.51 (1.52)	17.03 (0.21)
	30	60.34*** (4.08)	27.5*** (3.39)	5.96 (0.29)	3.93*** (0.84)
60	0.01	6.89 (1.56)	54.66*** (2.77)	9.37 (0.97)	24.54** (1.23)
	0.04	11.94** (1.41)	34.25*** (4.09)	17.95*** (2.5)	28.98*** (1.2)

induced apoptosis in 35.2% of the cells, methoxy-benzylidene **59** in 37.65% and indanocine (**10**) was responsible for an increase of 38.2 % on SKBR3 cancer cells. Based on these findings, it was understood that the cell cycle response did not change at 120 hrs independently of the substitution pattern of the benzylidene molecules used on SKBR3 cells.

3.2.2.6. Cell cycle effect of internal controls. Tamoxifen (**24**) showed a cell cycle arrest of SKBR3 at G0/G1 and S-phase at 24 hrs. However, differently from the findings observed by Ercoli and colleagues (Ercoli et al., 1998), tamoxifen (**24**) did not affect cell cycle of SKBR3 at 10 μM at 72 hrs. Nevertheless, at this time point we found a significant Sub-G0 arrest of cells (60.34%, $p < 0.001$) treated with 30 μM of tamoxifen. This result is consistent with the cytotoxicity we observed for tamoxifen on this cell line at 120 hrs, where 25.2 μM caused cell death in 50% of the treated cells. However, based on the results observed at 120 hrs we postulate that tamoxifen (**24**) did not induce programmed cell death in part of the cell population and the most resistant ones would keep proliferating, therefore decreasing proportionally the number of apoptotic cells at Sub-G0-phase.

Camptothecin (**60**) was introduced as a positive control at 72 hrs once indanocine was no longer available in the market. Camptothecin (**60**) class of compounds has been demonstrated to be effective against a broad spectrum of tumours. Cell treatment with Camptothecin has shown to induce DNA damage (Liu et al., 2000) *via* mitochondria-induced pathway (Li and Darzynkiewicz, 2000). Camptothecin at a dose that represents half of the IC_{50} on SKBR3 cells (0.01 μM) caused cycle arrest at G2/M ($p < 0.01$). An increase on the dose to two-fold its IC_{50} (0.04 μM) showed a statistically significant increment in both S and G2/M phase ($p < 0.001$) (Table 3 and Fig. 5). These results are in agreement with the literature data (Darzynkiewicz et al., 1996), where the most characteristic feature of camptothecin is its selective toxicity to DNA replicating cells. It has been said unclear, whether the delayed apoptosis seen at low camptothecin concentrations (3-60 nM), is selective to S phase cells, or whether the cells can complete DNA replication but die subsequently, following division. There is some evidence that such cells die in G1 phase of the cell cycle, which would suggest that the cells are able to divide, but they die in the subsequent cycle (reproductive or mitotic cell death).

3.2.2.7. Cell cycle effect of the hybrid compounds. The hybrid molecules **23, 47** and **49** were initially analysed at one single dose (10 μM) at 24 and 120 hrs. It was observed that among the hybrids, the unsubstituted molecule **23** demonstrated 2-fold higher apoptosis (Sub-G0) percentage at 24 hrs (6.39%) by comparison with indanocine (**10**) (2.37%) and tamoxifen (**24**) (3.58%). G2/M was strongly decreased at 120 hrs (9.78%) compared with 24 hrs (27.29%), when cells at Sub-G0 phase

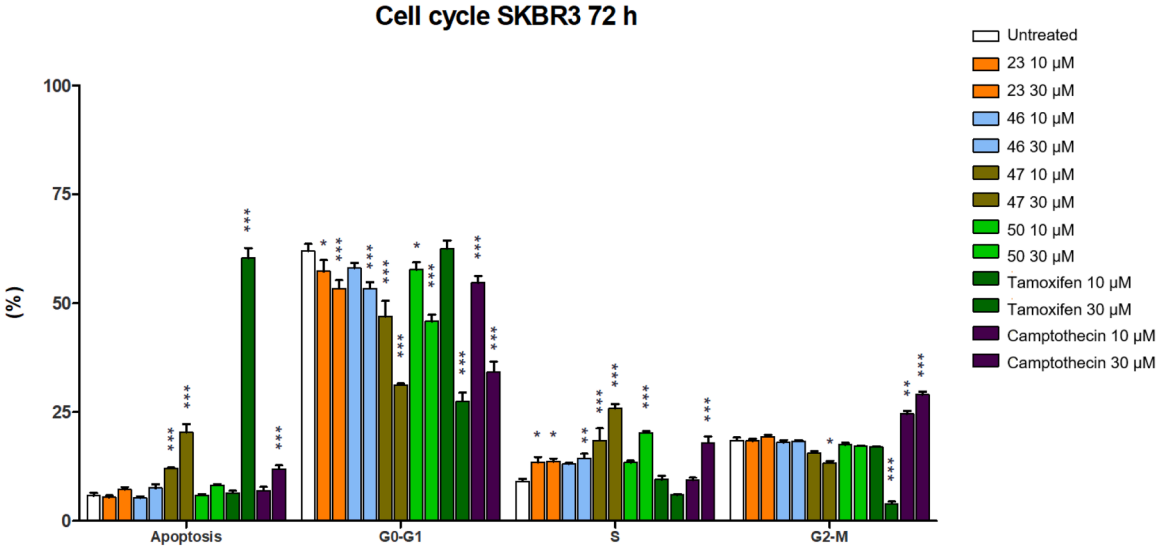

Fig. 5. Flow cytometry analysis determined the percentage of SKBR3 breast cancer cells in each cell cycle phase with respect to concentration of the treatments after 72 hrs exposure. The data represents the mean values after performing the experiment in triplicate with error bars indicating +SEM. Two-way ANOVA and Bonferroni posttest were used. *($p < 0.05$), **($p < 0.01$), ***($p < 0.001$).

reached 48.67 % of the cells analysed. After 24 hrs treatment, **49**, indanocine, methyl- and methoxy-benzylidenes did not affect cell cycle in SKBR3 cells. Tamoxifen showed a slight increase of 10% in G0-G1 in relation to negative control. Compound **23** demonstrated an initial alteration on cell cycle when compared with untreated cells. Interestingly, at 120 hrs indanocine was responsible for 38.2% of apoptosis while tamoxifen caused 27.71% on SKBR3 cancer cells (Fig. 4 and Table S4). The lead *p*-monosubstituted methyl hybrid **47** at 10 μM (nearly 10-fold higher its IC_{50} in SKBR3 cells) induced apoptosis in 26.89 % of the cells in 24 hrs. More surprisingly, this number went up to 90.56 % at 120 hrs (Fig. 4). The finding shows that besides being cytotoxic *in vitro* against the HER2+/Neu breast cancer cell line (SKBR3), **47** disturbs the replication and development of this type of cancer through a programmed cell death induction mechanism. Further studies were carried out and showed that the *p*-monosubstituted methyl hybrid **47** and the dimethyl derivative **50** arrested SKBR3 cells at 72 hrs in S-phase ($p < 0.001$) in a dose-dependent manner (Table 3 and Fig. 5). Compounds **23** ($p < 0.05$) and **46** ($p < 0.05$) followed the same pattern at 30 μM. It is known that DNA does not duplicate throughout the cycle but only during several hours in S-phase. Although S-phase is independent of growth factors, a massive DNA damage or deprivation of nucleotides forces a cell to be arrested in S-phase, and such arrest is usually accompanied by cell death (Blagosklonny and Pardee, 2002). Therefore, considering the results obtained (Fig. 5) we speculate DNA damage might be involved on the induction of SKBR3 cell death caused by these hybrid molecules. Compounds **23, 46, 47, 50**, tamoxifen (**24**) and camptothecin (**60**) demonstrated a dose dependent statistically significant decrease of cells in the G0/G1 phase of SKBR3 cell cycle (Fig. 5). The hybrids and camptothecin, on the other hand, also caused a significant increase of cells arrested at S phase. Tamoxifen (**24**) showed an opposite pattern despite the fact it was not statistically significant. Tamoxifen (**24**) has dose-dependently decreased the number of cells in G2/M, which was discretely observed only for the higher dose (30 μM) of the lead molecule **47**, with a lower intensity.

It is quite clear that the hybrid molecule **47** increased the percentage of cells at subG1 phase in a dose-dependent manner compared to the untreated control or other compounds at the same treated concentration. This indicates that the compound is more toxic against SKBR3 cells than other treatments. Although the percentage of cells treated with tamoxifen at the same concentration was significantly higher than all other treatments, including compound **47**, the population of cells at S-phase treated with compound **47** was higher than tamoxifen (**24**) or other compounds indicating that, while tamoxifen had a strong proapoptotic effect, compound **47** targeted DNA synthesis phase thus showed a higher cell cycle arrest potential than the indicated treatments. All the other molecules of this hybrid scaffold analysed did not change the cell cycle arrest at G2/M phase. Camptothecin, on the other hand, showed an opposite pattern once it dose-dependently arrested cells at G2/M phase (Fig. 5).

4. Conclusions

In conclusion, we designed and synthesised a new bioactive indane scaffold, 2-(diphenylmethylene)-2,3-dihydro-1H-inden-1-one, using two naturally derived ring systems: indane and benzophenone. The present work confirmed our working hypothesis that the hybridisation of indanone and benzophenone moieties yielded better analogues than the parent molecules in terms of their *in vitro* cytotoxicity against the four cancer cell lines investigated: MCF7 (breast) and SKBR3 (breast), DU145 (prostate) and A549 (lung). The methyl-, chloro- and methoxy-*para*-substituted benzophenone hybrids (**44**/**45, 46**/**47** and **48**/**49**) present a similar biological activity, displaying the greatest degree of cytotoxicity and the derivatives with the *E* configuration: **45, 47** and **49** being significantly most potent. In addition, it was demonstrated that the second benzyl functionality in the new scaffold is essential when compared to mono-substituted benzylidene indanones **59, 60** and **61**, especially against HER2+ breast cancer cells (SKBR3) by the *E*-methyl lead molecule **47**, in MCF7 (ER^+) by molecules **45** and **49**, and in the A549 (NSCLC) cell line by compound **49**. At this point, it is clear that different structural alterations render compounds more selective toward a specific cancerous cell line which necessitates further future studies including RNAseq to unravel the anti-proliferative mechanisms of the highly selective compounds. Another valuable aspect to study is how structural alterations can shift the selectivity of a compound from one cell type to another. For instance, the starting compound **22** showed no effect on SKBR3 and higher selectivity toward DU145 compared to other cell lines while hybrid **47** was more than 100-fold potent against SKBR3 and almost double the potency against DU 145 than the parent compound 22. Compound **47** was also 23 times more potent against SKBR3 than DU145 cell line. The finding of cell cycle analysis showed that besides being cytotoxic *in vitro* against SKBR3 cells the lead molecule **47** disturbs the replication and development of this type of cancer causing a dose-dependent cell cycle arrest at S-phase. We postulate that DNA damage might be involved on the induction of SKBR3 cell death caused by the hybrid molecules. The present study gives an insight into the pharmacological activity of this new chemical scaffold which has applicability in medicinal chemistry and may become a platform for new drug development given the effect observed. It points to potential structural optimisation of the series and encourages further focussed investigation of analogues of this scaffold series toward their applications in cancer chemoprevention or chemotherapy.

Appendix A. Supplementary data

Supplementary data to this article can be found online at:

CRediT authorship contribution statement

Tao Zhang: Methodology, Investigation, Writing – original draft, Writing – review & editing. **Vilmar Bandero:** Investigation, Writing – original draft, Writing – review & editing. **Claire Corcoran:** Investigation. **Ismael Obaidi:** Writing – review & editing. **Manuel Ruether:** Investigation. **John O'Brien:** Investigation. **Lorraine O'Driscoll:** Methodology, Investigation. **Neil Frankish:** Conceptualization, Investigation, Methodology. **Helen Sheridan:** Conceptualization, Methodology, Investigation, Writing – original draft, Writing – review & editing.

Declaration of Competing Interest

The authors declare that they have no known competing financial interests or personal relationships that could have appeared to influence the work reported in this paper.

Data availability

Data will be made available on request.

Acknowledgement

This work was supported by Trinity College Dublin Postgraduate Scholarships. The authors would like to thank Dr Brendan Twamley (School of Chemistry, Trinity College Dublin, Ireland) for preparing the x-ray crystallography data for this paper.

Supplementary materials

Supplementary material associated with this article can be found, in the online version, at doi:10.1016/j.ejps.2023.106529.

References

Ali, M.A., Choon, T.S., Lan, L.Y., Rosli, M.M., Fun, H.K., 2011. (E)-2-(4-Chloro-benzylidene)indan-1-one. Acta Crystallogr. Sect. E Struct. Rep. 67, o2064.

Aryanpour, N., Farnam, G., Behtaj, R, Shirazi, H.F., 2022. The complexity of response to the proliferation agonist and antagonist agents, in the breast cancer cell lines with various receptors. Iran. J. Pharm. Res. 16, e123823.
Asiri, A.M., Faidallah, H.M., Al-Nemari, K.F., Ng, S.W., Tiekink, E.R., 2012. (2E)-2-(4-Meth-oxy-benzyl-idene)-2,3-di-hydro-1H-inden-1-one. Acta Crystallogr. Sect. E Struct. Rep. 68, o815.
Barbosa, E.G., Bega, L.A.S., Beatriz, A., Sarkar, T., Hamel, E., do Amaral, M.S., de Lima, D.P., 2009. A diaryl sulfide, sulfoxide, and sulfone bearing structural similarities to combretastatin A-4. Eur. J. Med. Chem. 44, 2685–2688.
Biljali, S., Nedialkov, P., Zheleva-Dimitrova, D., Kitanov, G., Momekova, D., Momekov, G., 2013. Cytotoxic effects and multidrug resistance modulation by five benzophenones and a xanthone isolated from Hypericum annulatum moris subsp. annulatum. Biotechnol. Biotechnol. Equip. 27, 3561–3568.
Blagosklonny, M.V., Pardee, A.B., 2002. The restriction point of the cell cycle. Cell Cycle 1, 103–110.
Bruker, 2014. XPREP. Bruker-AXS, Madison, WI, USA.
Chan, K., Frankish, N., Zhang, T., Ece, A., Cannon, A., O'Sullivan, J., Sheridan, H., 2020. Bioactive indanes: insight into the bioactivity of indane dimers related to the lead anti-inflammatory molecule PH46A. J. Pharm. Pharmacol. 72, 927–937.
Collins, K., Jacks, T., Pavletich, N.P., 1997. The cell cycle and cancer. Proc. Natl. Acad. Sci 94, 2776–2778.
Coyanis, E.M., Panayides, J.-L., Fernandes, M.A., de Koning, C.B., van Otterlo, W.A.L., 2006. Ring-closing metathesis for the synthesis of substituted indenols, indenones, indanones and indenes: Tandem RCM-dehydrogenative oxidation and RCM-formal redox isomerization. J. Organomet. Chem. 691, 5222–5239.
Darzynkiewicz, Z., Bruno, S., Del Bino, G., Traganos, F., 1996. The cell cycle effects of camptothecin. Ann. N. Y. Acad. Sci. 803, 93–100.
Dolomanov, O.V., Bourhis, L.J., Gildea, R.J., Howard, J.A.K., Puschmann, H., 2009. OLEX2: a complete structure solution, refinement and analysis program. J. Appl. Crystallogr. 42, 339–341.
Dressing, G.E., Alyea, R., Pang, Y.F., Thomas, P., 2012. Membrane progesterone receptors (mPRs) mediate progestin induced antimorbidity in breast cancer cells and are expressed in human breast tumors. Horm. Cancer 3, 101–112.
Elmore, S., 2007. Apoptosis: A review of programmed cell death. Toxicol. Pathol. 35, 495–516.
Ercoli, A., Scambia, G., Fattorossi, A., Raspaglio, G., Battaglia, A., Cicchillitti, L., Malorni, W., Rainaldi, G., Benedetti Panici, P., Mancuso, S., 1998. Comparative study on the induction of cytostasis and apoptosis by ICI 182,780 and tamoxifen in an estrogen receptor-negative ovarian cancer cell line. Int. J. Cancer 76, 47–54.
Erhan, S., 2008. Synthesis of cyclic acetals (ketals) from oleochemicals using a solvent free method. Green Chem 10.
Ferris, R.G., Hazen, R.J., Roberts, G.B., St. Clair, M.H., Chan, J.H., Romines, K.R., Freeman, G.A., Tidwell, J.H., Schaller, L.T., Cowan, J.R., 2005. Antiviral activity of GW678248, a novel benzophenone nonnucleoside reverse transcriptase inhibitor. Antimicrob. Agents Chemother. 49, 4046–4051.
Ferraz, C.G., Ribeiro, P.R., Mendonça, R., Silveira, E.R., Cruz, F.G., 2021. Novel polyprenylated benzophenone derivatives from Clusia burle-marxii. Fitoterapia 149, 104760.
Frampton, C.S., Zhang, T., Scalabrino, G.A., Frankish, N., Sheridan, H., 2012. 1S)-1-Phenylethanaminium 4-{[(1S,2S)-1-hydroxy-2,3-dihydro-1H,1′H-[2,2′-biinden]-2-yl]methyl}benzoate. Acta Crystallogr. C. 68, o323–o326.
Frankish, N., Farrell, R., Sheridan, H., 2004. Investigation into the mast cell stabilizing activity of nature-identical and synthetic indanones. J. Pharm. Pharmacol. 56, 1423–1427.
Frankish, N., Sheridan, H., 2012. 6-(Methylamino)hexane-1,2,3,4,5-pentanol 4-(((1S,2S)-1-Hydroxy-2,3-dihydro-1H,1′H-[2,2-biinden]-2-yl)methyl)benzoate (PH46A): A novel small molecule with efficacy in murine models of colitis. J. Med Chem. 55, 5497–5505.
Frankish, N.H., McHale, B., Sheridan, H., 2017. The indane diastereoisomers, PH2 and PH5: divergence between their effects in delayed-type hypersensitivity models and a model of colitis. J. Pharm. Pharmacol. 70, 101–110.
Ghinet, A., Rigo, B., Hénichart, J.P., Le Broc-Ryckewaert, D., Pommery, J., Pommery, N., Thuru, X., Quesnel, B., Gautret, P., 2011. Synthesis and biological evaluation of phenstatin metabolites. Bioorg. Med. Chem. 19, 6042–6054.
Godyń, J., Zaręba, P., Stary, D., Kaleta, M., Kuder, K.J., Latacz, G., Mogilski, S., Reiner-Link, D., Frank, A., Doroz-Płonka, A., Olejarz-Maciej, A., Sudoł-Tałaj, S., Nolte, T., Handzlik, J., Stark, H., Więckowska, A., Malawska, B., Kieć-Kononowicz, K., Łażewska, D., Bajda, M., 2022. Benzophenone derivatives with histamine H(3) receptor affinity and cholinesterase inhibitory potency as multitarget-directed ligands for possible therapy of Alzheimer's disease. Molecules 28.
Hajduk, P.J., Bures, M., Praestgaard, J., Fesik, S.W., 2000. Privileged molecules for protein binding identified from NMR-based screening. J. Med. Chem. 43, 3443–3447.
Hevir, N., Trošt, N., Debeljak, N., Rižner, T.L., 2011. Expression of estrogen and progesterone receptors and estrogen metabolizing enzymes in different breast cancer cell lines. Chem. Biol. Interact. 30, 206–216.
Holliday, D.L., Speirs, V., 2011. Choosing the right cell line for breast cancer research. Breast Cancer Res. 13, 215.
Jaki, B., Orjala, J., Bürgi, H.R., Sticher, O., 1999. Biological screening of cyanobacteria for antimicrobial and molluscicidal activity, brine shrimp lethality, and cytotoxicity. Pharm. Biol. 37, 138–143.
Kamal, A., Kumar, G.B., Vishnuvardhan, M.V.P.S., Shaik, A.B., Reddy, V.S., Mahesh, R., Sayeeda, I.B., Kapure, J.S., 2015. Synthesis of phenstatin/isocombretastatin–chalcone conjugates as potent tubulin polymerization inhibitors and mitochondrial apoptotic inducers. Org. Biomol. Chem. 13, 3963–3981.
Kim, S.-H., Kwon, S.H., Park, S.-H., Lee, J.K., Bang, H.-S., Nam, S.-J., Kwon, H.C., Shin, J., Oh, D.-C., 2013. Tripartin, a histone demethylase inhibitor from a bacterium associated with a dung beetle larva. Org. Lett. 15, 1834–1837.
Kou, X., Shen, K., An, Y., Qi, S., Dai, W.X., Yin, Z., 2012. Ampelopsin inhibits H_2O_2-induced apoptosis by ERK and Akt signaling pathways and up-regulation of heme oxygenase-1. Phytother. Res. 26, 988–994.
Kumar, P., Shirke, R.P., Yadav, S., Ramasastry, S.S.V., 2021. Catalytic enantioselective synthesis of axially chiral diarylmethylidene indanones. Org. Lett. 23, 4909–4914.
Lant, A.F., 1981. Modern diuretics and the kidney. J. Clin. Pathol. 34, 1267.
Leoni, L.M., Hamel, E., Genini, D., Shih, H., Carrera, C.J., Cottam, H.B., Carson, D.A., 2000. Indanocine, a microtubule-binding indanone and a selective inducer of apoptosis in multidrug-resistant cancer cells. J. Natl. Cancer Inst. 92, 217–224.
Li, X., Darzynkiewicz, Z., 2000. Cleavage of Poly(ADP-ribose) polymerase measured in situ in individual cells: relationship to DNA fragmentation and cell cycle position during apoptosis. Exp. Cell Res. 255, 125–132.
Liu, L.F., Desai, S.D., Li, T.K., Mao, Y., Sun, M., Sim, S.P., 2000. Mechanism of action of camptothecin. Ann. N.Y. Acad. Sci. 922, 1–10.
Lukács, G., Porcs-Makkay, M., Komáromi, A., Simiga, G., 2008. Microwave assisted synthesis of benzophenone and acetophenone ethylene ketals. Arkivoc 17–24, 2008.
Lukács, G., Porcs-Makkay, M., Simig, G., 2004. Lithiation of 2-aryl-2-(chloroaryl)-1,3-dioxolanes and its application in the synthesis of new ortho-functionalized benzophenone derivatives. Eur. J. Org. Chem. 4130–4140, 2004.
Maciel-Rezende, C.M., de Almeida, L., Costa É, D., Pires, F.R., Alves, K.F., Viegas Jr., C., Dias, D.F., Doriguetto, A.C., Marques, M.J., dos Santos, M.H., 2013. Synthesis and biological evaluation against Leishmania amazonensis of a series of alkyl-substituted benzophenones. Bioorg. Med. Chem. 21, 3114–3119.
Martin, A., Clynes, M., 1993. Comparison of 5 microplate colorimetric assays for in vitro cytotoxicity testing and cell proliferation assays. Cytotechnology 11, 49–58.
Muler, M., Antunes, Fernanda A., Guarache, G.C., Oliveira, R.B., Ureshino, R.P., Bincoletto, C., Pereira, G.J.S., Smaili, S.S., 2020. Effects of ICI 182,780, an ERα and ERβ antagonist, and G-1, a GPER agonist, on autophagy in breast cancer cells. Einstein (São Paulo) 18, eAO4560.
Nord, C.L., Menkis, A., Lendel, C., Vasaitis, R., Broberg, A., 2014. Sesquiterpenes from the saprotrophic fungus Granulobasidium vellereum (Ellis & Cragin) Jülich. Phytochemistry 102, 197–204.
Pettit, G.R., Grealish, M.P., Herald, D.L., Boyd, M.R., Hamel, E., Pettit, R.K., 2000. Antineoplastic agents. 443. Synthesis of the cancer cell growth inhibitor hydroxyphenstatin and its sodium diphosphate prodrug. J. Med. Chem. 43, 2731–2737.
Pettit, G.R., Toki, B., Herald, D.L., Verdier-Pinard, P., Boyd, M.R., Hamel, E., Pettit, R.K., 1998. Antineoplastic agents. 379. Synthesis of phenstatin phosphate. J. Med. Chem. 41, 1688–1695.
Pucci, B., Kasten, M., Giordano, A., 2000. Cell cycle and apoptosis. Neoplasia 2, 291–299.
Rigaku, 2006. CrystalClear. Rigaku Corporation, Tokyo, Japan.
Sharaf, B.M., Giddey, A.D., Alniss, H., Al-Hroub, H.M., El-Awady, R., Mousa, M., Almehdi, A., Soares, N.C., Semreen, M.H., 2022. Untargeted metabolomics of breast cancer cells MCF-7 and SKBr3 treated with tamoxifen/trastuzumab. Cancer Genomics Proteomics 19, 79–93.
Sheldrick, G.M., 2008. A short history of SHELX. Acta Crystallogr.-Foundation Adv. 64, 112–122.
Sheldrick, G.M., 2015. Crystal structure refinement with SHELXL. Acta Crystallogr. C Struct. Chem. 71, 3–8.
Sheridan, H., Walsh, J.J., Cogan, C., Jordan, M., McCabe, T., Passante, E., Frankish, N.H., 2009. Diastereoisomers of 2-benzyl-2, 3-dihydro-2-(1H-inden-2-yl)-1H-inden-1-ol: potential anti-inflammatory agents. Bioorg. Med. Chem. Lett. 19, 5927–5930.
Thompson, E.W., Reich, R., Shima, T.B., Albini, A., Graf, J., Martin, G.R., Dickson, R.B., Lippman, M.E., 1988. Differential regulation of growth and invasiveness of MCF-7 breast cancer cells by antiestrogens1. Cancer Res 48, 6764–6768.
Tzanova, T., Gerova, M., Petrov, O., Karaivanova, M., Bagrel, D., 2009. Synthesis and antioxidant potential of novel synthetic benzophenone analogues. Eur. J. Med. Chem. 44, 2724–2730.
Weißenborn, C., Ignatov, T., Poehlmann, A., Wege, A.K., Costa, S.D., Zenclussen, A.C., Ignatov, A., 2014. GPER functions as a tumor suppressor in MCF-7 and SK-BR-3 breast cancer cells. J. Cancer Res. Clin. Oncol. 140, 663–671.
Wu, M., Ji, Q., Yang, C., Xie, Y., 2005. A novel and convenient method for the synthesis of phenstatin. Org. Prep. and Proced. Int. 37, 272–275.
Wu, S.B., Long, C., Kennelly, E.J., 2014. Structural diversity and bioactivities of natural benzophenones. Nat. Prod. Rep. 31, 1158–1174.
Xue, C.B., Chen, L., Cao, G., Zhang, K., Wang, A., Meloni, D., Glenn, J., Anand, R., Xia, M., Kong, L., Huang, T., Feng, H., Zheng, C., Li, M., Galya, L., Zhou, J., Shin, N., Baribaud, F., Solomon, K., Scherle, P., Zhao, B., Diamond, S., Emm, T., Keller, D., Contel, N., Yeleswaram, S., Vaddi, K., Hollis, G., Newton, R., Friedman, S., Metcalf, B., 2010. Discovery of INCB9471, a potent, selective, and orally bioavailable CCR5 antagonist with potent anti-HIV-1 activity. ACS Med. Chem. Lett. 1, 483–487.
Yang, F., Jin, T., Yamamoto, Y., 2012. Synthesis of 2,3-dihydro-1H-inden-1-one derivatives via Ni-catalyzed intramolecular hydroacylation. Tetrahedron 68, 5223–5228.
Zeng, H.T., Yu, Y.H., Zeng, X., Li, M.M., Li, X., Xu, S.S., Tu, Z.C., Yuan, T., 2022. Anti-inflammatory dimeric benzophenones from an endophytic pleosporales species. J. Nat. Prod. 85, 162–168.
Zhang, T., Bandero, V., McCabe, T., Frankish, N., Sheridan, H., 2013. 2-(Di-phenyl-methyl-idene)-2,3-di-hydro-1H-inden-1-one. Acta Crystallogr. Sect. E Struct. Rep. 69, o1306–o1307.

Zhang, T., Paluch, K., Scalabrino, G., Frankish, N., Healy, A.M., Sheridan, H., 2015. Molecular structure studies of (1S,2S)-2-benzyl-2,3-dihydro-2-(1H-inden-2-yl)-1H-inden-1-ol. J. Mol. Struct. 1083, 286–299.
Zhang, T., Twamley, B., Sheridan, H., 2014. 2-(Diphenylmethylidene)-2,3-dihydro-1H-inden-1-one, 02 May 2014 ed. Cambridge Crystallographic Data Centre.
Zhou, N.-N., Ning, S.-S., Tong, X.-J., Luo, T.-T., Yang, J., Li, L.-Q., Fan, M.-J., Yang, D.-S., Zhu, H.-T., 2019. Brønsted-acid-catalyzed synthesis of 3-alkoxy and 3-sulfamido indanones via a tandem cyclization. J. Org. Chem. 84, 8497–8508.
Zhou, Y., 2019. CCDC 1910648: Experimental Crystal Structure Determination. Cambridge Crystallographic Data Centre. CSD Communication.
Zou, G., Li, T.B., Yang, W.C., Sun, B., Chen, Y., Wang, B., Ou, Y.H., Yu, H.J., She, Z.G., 2023. Antioxidative indenone and benzophenone derivatives from the mangrove-derived fungus Cytospora heveae NSHSJ-2. Mar. Drugs 21, 1–10.